Discovery of novel berberine derivatives with balanced cholinesterase and prolyl oligopeptidase inhibition profile

Katerina Sobolova, Martina Hrabinova, Vendula Hepnarova, Tomas Kucera, Tereza Kobrlova, Marketa Benkova, Jana Janockova, Rafael Dolezal, Lukas Prchal, Ondrej Benek, Eva Mezeiova, Daniel Jun, Ondrej Soukup, Jan Korabecny

PII: S0223-5234(20)30565-1

DOI: https://doi.org/10.1016/j.ejmech.2020.112593

Reference: EJMECH 112593

To appear in: *European Journal of Medicinal Chemistry*

Received Date: 16 May 2020

Revised Date: 15 June 2020

Accepted Date: 15 June 2020

Please cite this article as: K. Sobolova, M. Hrabinova, V. Hepnarova, T. Kucera, T. Kobrlova, M. Benkova, J. Janockova, R. Dolezal, L. Prchal, O. Benek, E. Mezeiova, D. Jun, O. Soukup, J. Korabecny, Discovery of novel berberine derivatives with balanced cholinesterase and prolyl oligopeptidase inhibition profile, *European Journal of Medicinal Chemistry*, https://doi.org/10.1016/j.ejmech.2020.112593.

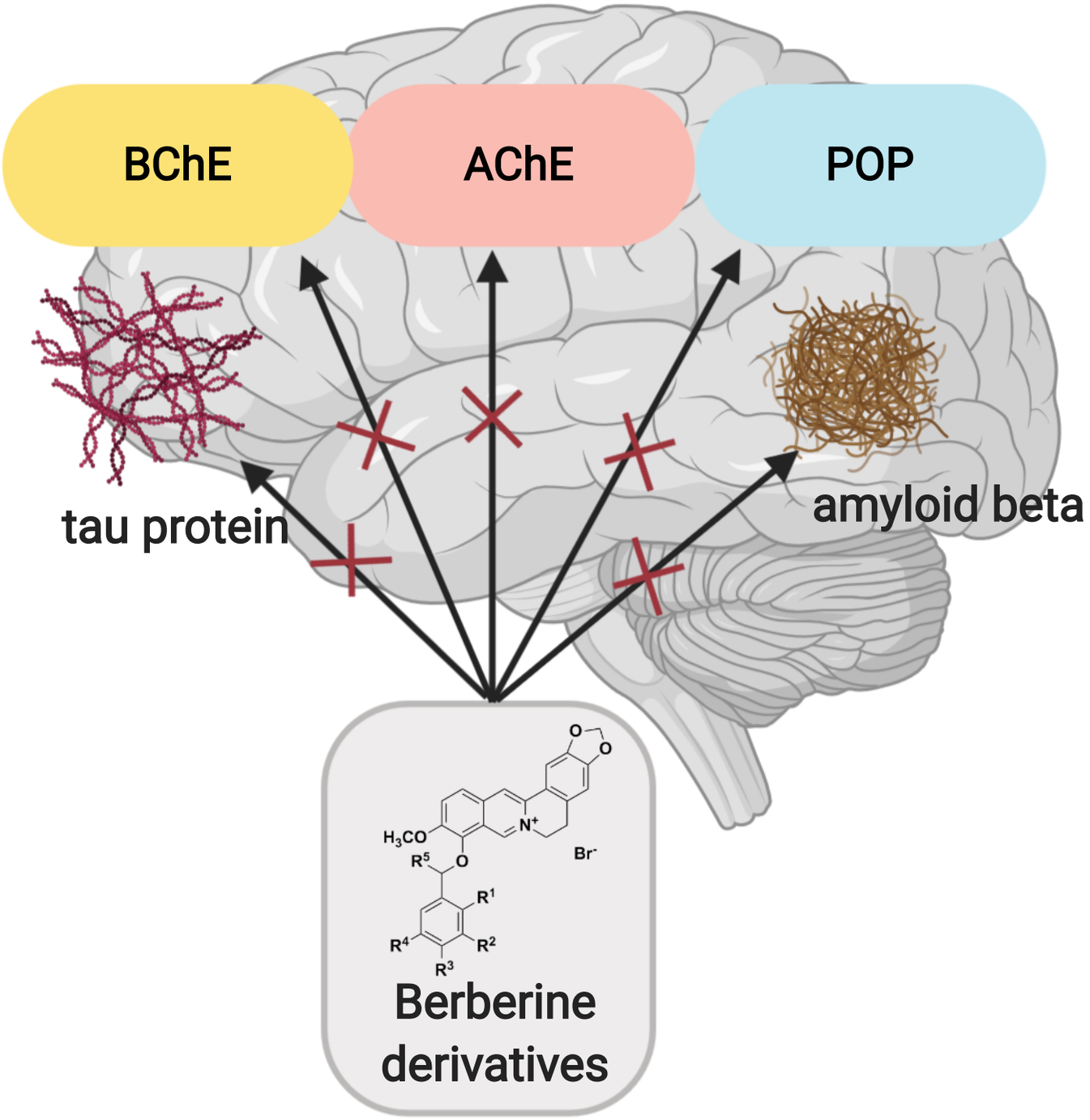
BChE
AChE
POP
tau protein
amyloid beta
Berberine
derivatives

Discovery of novel berberine derivatives with balanced cholinesterase and prolyl oligopeptidase inhibition profile

Katerina Sobolova[1,#], Martina Hrabinova[1,2,#], Vendula Hepnarova[1], Tomas Kucera[1], Tereza Kobrlova[1,2], Marketa Benkova[2], Jana Janockova[2], Rafael Dolezal[2,3], Lukas Prchal[2], Ondrej Benek[2], Eva Mezeiova[2], Daniel Jun[1,2], Ondrej Soukup[1,2,*], Jan Korabecny[1,2,*]

[1] *Department of Toxicology and Military Pharmacy, Department of Military Medical Service Organisation and Management; Faculty of Military Health Sciences, University of Defense, Trebesska 1575, 500 05 Hradec Kralove, Czech Republic*

[2] *Biomedical Research Centre, University Hospital Hradec Kralove, Sokolska 581, 500 05 Hradec Kralove, Czech Republic*

[3] *Department of Chemistry, Faculty of Science, University of Hradec Kralove, Rokitanskeho 62, 500 03 Hradec Kralove, Czech Republic*

[#] equal contribution

*** corresponding authors:** Ondrej Soukup: Phone: +420 495 833 447; E-mail: ondrej.soukup@fnhk.cz; Jan Korabecny: Phone: +420 495 833 447; E-mail: jan.korabecny@fnhk.cz

ABSTRACT

Berberine, a naturally occurring compound, possesses an interesting multipotent pharmacological profile potentially applicable for Alzheimer´s disease (AD) treatment. In this study, a series of novel 22 berberine derivatives was developed and tested *in vitro*. Berberine core was substituted at position 9-*O* of its aromatic ring region. All the hybrids under the study revealed multi-targeted profile inhibiting prolyl oligopeptidase, acetylcholinesterase and butyrylcholinesterase highlighting **4a**, **4g**, **4j**, **4l** and **4s** possessing balanced activities in the micromolar range. The top-ranked candidates in terms of the most pronounced potency against POP, AChE and BChE can be classified as **4d**, **4u** and **4v**, bearing 4-methylbenzyl, (naphthalen-2-yl)methylene and 1-phenoxyethyl moieties, respectively. *In vitro* data were corroborated by detailed kinetic analysis of the selected lead molecules. **4d**, **4u** and **4v** were also inspected for their potential to inhibition aggregation of two abberant proteins in AD, namely amyloid beta and tau, indicating their potential disease-modifying properties. To explain the results of our study, we carried out docking simulation to the active sites of the respective enzyme with the best berberine derivatives, along with QSAR study. We also investigated compounds' potential permeability through blood-brain barrier by applying parallel artificial membrane permeation assay and addressed their cytotoxicity profile.

KEYWORDS: acetylcholinesterase; Alzheimer´s disease; amyloid beta; butyrylcholinesterase; in silico; multi-target directed ligands; prolyl oligopeptidase; quantitative structure-activity relationship; tau protein

1. INTRODUCTION

Alzheimer´s disease (AD) is a type of dementia that causes a decline in intellectual and functional abilities [1]. As of 2019, the global prevalence of AD is estimated to be as high as 50 million, foreseeing that the number of AD patients can exceed 152 milion by 2050 [2]. One of the greatest known risk factors is increasing age, since the majority of people suffering from AD are older than 65. From a neurobiological point of view, AD is a chronic neurodegenerative disorder of the brain characterized by loss of neurons and synapses in the medial temporal lobe and neocortical association areas. The atrophy of these brain regions manifests as memory impairment, difficulty in learning, loss of language skills, not managing the daily self-care, disorientation and personality changes [3].

AD can be considered as a multifactorial and complex disorder with prevailing deficits in cholinergic system, changes in prolyl oligopeptidase (POP; E.C. 3.4.21.26) activity, elevated levels of reactive oxygen species (ROS), presence of aberrant proteins like amyloid-beta peptide (Aβ) forming neuritic plaques and intracellular neurofibrillary tangles composed of hyperphosphorylated tau (τ) protein. That all leads to neuronal death and clinical manifestations of this disease [4–6]. One of the typical phenomenon associated with AD is cellular oxidative and nitrosative stress, which is responsible for dysregulation of nucleic acids and proteins formation, lipid peroxidation and glycoxidation [7]. Oxidative stress (OS) is the culprit of metabolic, metal, mitochondrial and cell-cycle abnormalities. Mitochondria are regulators of cell death, and therefore mutations in their DNA together with OS contribute to aging [8,9]. The intervention strategies comprise the use of effective antioxidants, up-regulation of the endogenous antioxidative defense system, and administration of anti-inflammatory agents as well. Apart from that, it is also well established that monoamine oxidases are involved in the production of hydrogen peroxide; thus, their inhibitors may ameliorate damages associated with OS [10,11].

Current palliative treatment is based on the administration of acetylcholinesterase (AChE; E.C. 3.1.1.7) inhibitors as the most pronounced pathology in AD is associated with cholinergic neuronal loss. There has also been confirmed interconnection between disrupted cholinergic system and the formation of intracellular neurofibrillary tangles or senile plaques [1,12]. For instance, Inestrosa group found that AChE acts as a pathological chaperone inducing a conformational transition of Aβ [13]. Generally, the cholinergic hypothesis claims that the lack of the acetylcholine (ACh) neurotransmitter in the cortex is responsible for

cognitive decline. Both AChE and butyrylcholinesterase (BChE; E.C. 3.1.1.8) are responsible for the breakdown of ACh in the synapses [14]. The progression of AD goes hand in hand with AChE activity decrease, which is counterbalanced at the same time by BChE increase [14,15]. Therefore inhibition of both cholinesterases (ChEs) can elevate ACh levels and thus mitigate AD symptoms.

There are a number of experimental targets that popped-up recently as the promising ones, which are involved in the pathophysiology of the disease, and their targeting might result in complex action in the disease cascade. One such target is POP enzyme, the cytosolic serine peptidase. POP is implicated in physiological processes such as maturation and degradation of peptide hormones and neuropeptides, such as substance P, thymosin β4, thyrotropin-releasing hormone, vasopressin, and angiotensin. POP inhibitors (POPi) may improve memory impairment by blocking the metabolism of these substrates. Therefore, POP has been proposed as a potential therapeutic target for several disorders as, rheumatoid arthritis [16,17], cystic fibrosis [18], α-synucleinopathies [19], AD [20], autism spectrum disorder [21], cirrhosis [22], mania and schizophrenia [23], and high POP activity was observed in proliferating cells [24]. Surprisingly, suppressed expression of POP by an antisense technique and by specific POPi revealed an inverse correlation between inositol 1, 4, 5-triphosphate (Ins(1, 4, 5)P_3) concentration. Furthermore, decreased activity of POP amplifies substance P mediated stimulation of Ins(1, 4, 5)P_3, which is the intracellular second messenger that binds to its receptor located in the membrane of the endoplasmatic reticulum and induces release of Ca^{2+} which may have an impact on cognitive enhancements. These findings can explain a relationship between an intracellular enzyme such as POP and the neuropeptides, because Ins(1, 4, 5)P_3 is a central molecule in the signaling cascade of neuropeptides [25]. Promising results were reported for some POPi in clinical trials. However, these were terminated mostly due to unfavorable pharmacokinetic profile of the compounds [26].

Searching for new AD therapeutic options remains an elusive task. Given the complexity of the disorder, applying a multi-target drug discovery approach might deliver more effective therapeutics [27–29]. Indeed, this strategy foresees to target different enzymes/receptors at the same time that may ultimately better address the needs to find a novel and effective cure. One such option represents the chemical modification of natural compounds to improve their pharmacological activities. Berberine (BBR; Fig. 1), a quaternary

ammonium protoberberine alkaloid, has been used in traditional Chinese and Ayurvedic medicine possessing a broad spectrum of pharmacological properties. Some of the BBR analogs have already been investigated in clinical trials [30].

Within this study, we inspected the structure-activity relationship (SAR) in the series of novel BBR derivatives substituted in position 9-*O* with different aromatic rings. We tested the novel compounds for the inhibition of ChEs and POP enzymes, their potency to counteract OS and we predicted their capacity to cross the blood-brain barrier (BBB). For the highlighted derivatives, we also performed anti-amyloid and anti-tau studies, and predicted their binding modes in the active sites of the respective enzymes.

2. DESIGN

The nature of AD assumes that the therapeutic intervention can be successfully pursued by small molecules hitting multiple targets relevant to the disorder simultaneously. Berberine (BBR) is a natural isoquinoline alkaloid with an intrinsic multipotent profile [7]. Indeed, BBR shows antioxidative, anti-proliferative, anti-inflammatory, amyloid-β (Aβ) peptide level-reducing, monoamine oxidase, and cholinesterase inhibitory activities [31–33]. It has also been described that BBR improves cognitive impairment by inhibiting abnormal Aβ aggregation and τ hyperphosphorylation [34]. Moreover, it ameliorates OS and neuroinflammation [35]. Its neuroprotective properties were also confirmed in metal-induced neurotoxicity animal models of AD [36]. BBR displayed dose-dependent POP inhibition properties with IC_{50} = 145 μM [37]. Inhibition of both enzymes (AChE and POP) potentiates resultant of cognitive effect whereas POP inhibition leads, due to enhanced Ins(1, 4, 5)P_3 levels, to similar mechanism as signalization at muscarinic ACh receptor M_1 [38].

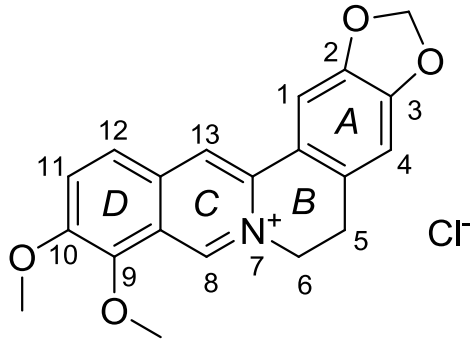

Figure 1. Chemical structure of berberine with numbering of the core scaffold.

BBR is endowed with a broad pharmacologic profile, on one hand; on the other hand, it is hampered by relatively low permeability and bioavailability due to its hydrophilic character that limits its systematic administration [30]. For these reasons, structural modifications increasing BBR lipophilicity, mostly in position 9-, are pursued in order to address these drawbacks [39–42]. From the wealth of literature, several SAR were outlined. For example, SAR analysis in 9-*N*-alkyl-substituted BBR derivatives indicated higher antioxidant and Aβ anti-aggregation properties [43]. Furthermore, attachment of lipophilic substituent to BBR in the region of methylenedioxy substituted aromatic ring, and methoxyl moiety at C-10 indicated increased hypoglycemic activity [44]. The introduction of aminomethyl groups into 12-position of berberrubine improved the insulin-resistant reversal activity and stimulated glucose transport activity, which is potentially applicable for type 2 diabetes mellitus (T2DM) [45]. Indeed, a growing body of epidemiological studies suggest that people with T2DM are at a higher risk of developing AD [46]. For cholesterol-lowering and anti-diabetic agents, it have been observed that methylenedioxy functionality in BBR orchestrates binding to β-cell membranes [47–50]. Accordingly, BBR and its derivatives may reduce the risk factors associated with AD, i.e. high levels of glucose and cholesterol.

Building on the findings above, in this study, we are exploring SAR in 9-subsitited BBR derivatives. Into this position, we attached different lipophilic substituents to enhance permeability through cell membranes plausibly. In parallel, 9-*N* substituted BBR derivatives synthesized by Shan and colleagues [43] showed promising results as antioxidants; AChE, BuChE and Aβ aggregation inhibitors but 9-*O* substitution, to the best of our knowledge, was not tested for the possible cognitive enhancing properties. Herewith, we designed and synthesized a new family of compounds based on nucleophilic substitution at 9-*O*- position of BBR core.

3. RESULTS AND DISCUSSION

3.1 Chemistry

BBR derivatives were synthesized following a chemical procedure depicted in Scheme 1. Initially, BBR (**1**) chloride underwent demethylation at position 9- in a vacuum (15 mbar) at 205 °C for 2 hours which was clearly visible by a color change from yellow to dark red forming berberrubine (**2**; 77% yield) [51]. Berberrubine was then treated with potassium carbonate in anhydrous MeCN at 80 °C for 30 min followed by the addition of appropriate

benzyl bromide (**3a**-**3v**) and the mixture was refluxed for 1 h at 80 °C. Only reagent **3b** was dissolved in a mixture of anhydrous solvents THF/MeCN (1:1) because of its low solubility in sole MeCN. To generate **4v**, we used 2-(bromomethyl)naphthalene (**3v**) under the same conditions. After cooling, the reaction mixture was filtered and washed successively with MeCN (50 mL) and MeOH (50 mL). Column chromatography was used for purification to produce **4a**-**4v** in 8-91% yields. All of the final compounds **4a**-**4v** showed analytical and spectroscopic data in good agreement with their structures. Structural characterization involved melting points, ^{1}H and ^{13}C NMR spectra, and LC−MS analysis. All the ^{1}H and ^{13}C NMR spectra can be found at Supplementary information.

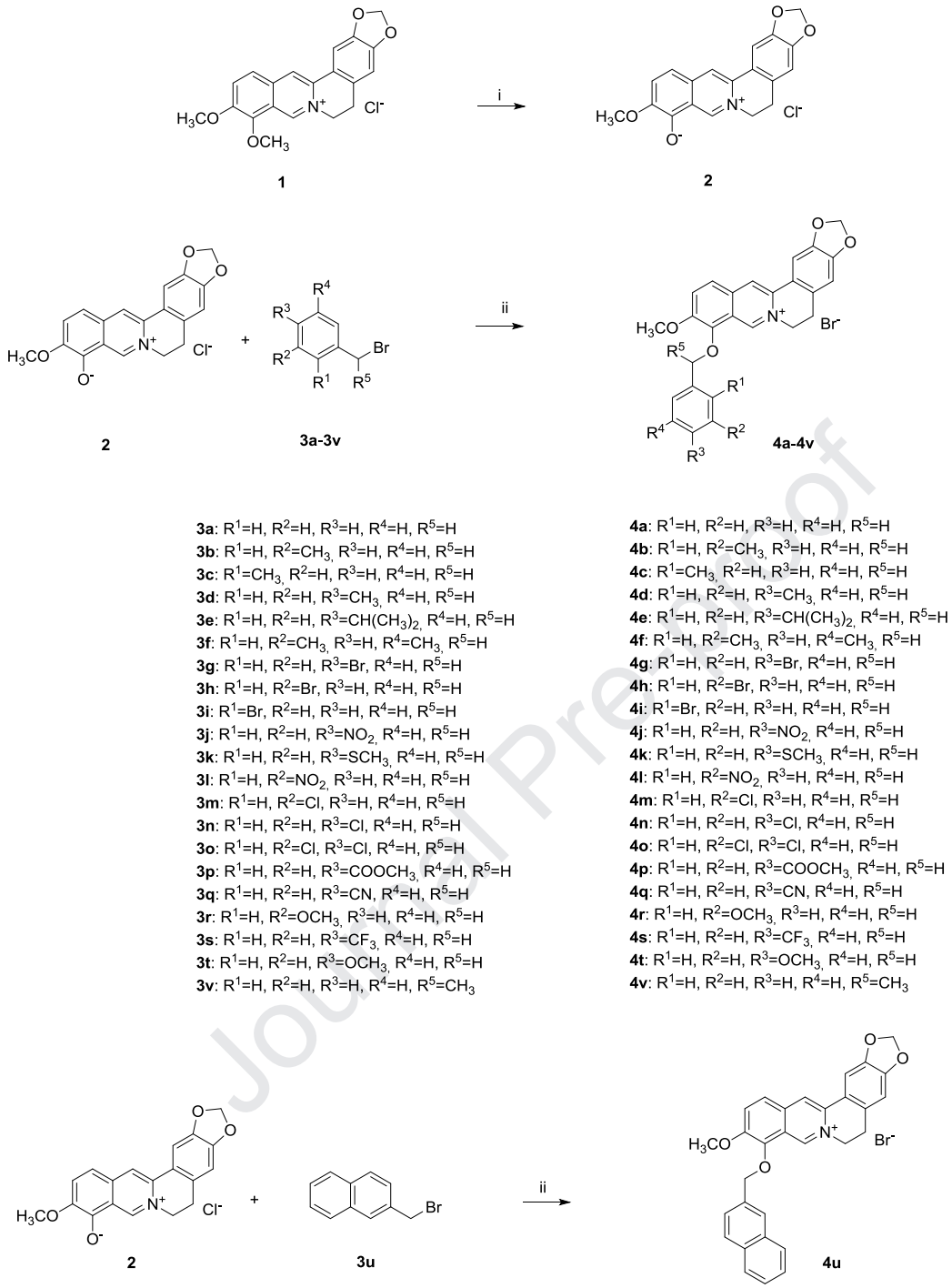

3a: R^1=H, R^2=H, R^3=H, R^4=H, R^5=H
3b: R^1=H, R^2=CH_3, R^3=H, R^4=H, R^5=H
3c: R^1=CH_3, R^2=H, R^3=H, R^4=H, R^5=H
3d: R^1=H, R^2=H, R^3=CH_3, R^4=H, R^5=H
3e: R^1=H, R^2=H, R^3=$CH(CH_3)_2$, R^4=H, R^5=H
3f: R^1=H, R^2=CH_3, R^3=H, R^4=CH_3, R^5=H
3g: R^1=H, R^2=H, R^3=Br, R^4=H, R^5=H
3h: R^1=H, R^2=Br, R^3=H, R^4=H, R^5=H
3i: R^1=Br, R^2=H, R^3=H, R^4=H, R^5=H
3j: R^1=H, R^2=H, R^3=NO_2, R^4=H, R^5=H
3k: R^1=H, R^2=H, R^3=SCH_3, R^4=H, R^5=H
3l: R^1=H, R^2=NO_2, R^3=H, R^4=H, R^5=H
3m: R^1=H, R^2=Cl, R^3=H, R^4=H, R^5=H
3n: R^1=H, R^2=H, R^3=Cl, R^4=H, R^5=H
3o: R^1=H, R^2=Cl, R^3=Cl, R^4=H, R^5=H
3p: R^1=H, R^2=H, R^3=$COOCH_3$, R^4=H, R^5=H
3q: R^1=H, R^2=H, R^3=CN, R^4=H, R^5=H
3r: R^1=H, R^2=OCH_3, R^3=H, R^4=H, R^5=H
3s: R^1=H, R^2=H, R^3=CF_3, R^4=H, R^5=H
3t: R^1=H, R^2=H, R^3=OCH_3, R^4=H, R^5=H
3v: R^1=H, R^2=H, R^3=H, R^4=H, R^5=CH_3

4a: R^1=H, R^2=H, R^3=H, R^4=H, R^5=H
4b: R^1=H, R^2=CH_3, R^3=H, R^4=H, R^5=H
4c: R^1=CH_3, R^2=H, R^3=H, R^4=H, R^5=H
4d: R^1=H, R^2=H, R^3=CH_3, R^4=H, R^5=H
4e: R^1=H, R^2=H, R^3=$CH(CH_3)_2$, R^4=H, R^5=H
4f: R^1=H, R^2=CH_3, R^3=H, R^4=CH_3, R^5=H
4g: R^1=H, R^2=H, R^3=Br, R^4=H, R^5=H
4h: R^1=H, R^2=Br, R^3=H, R^4=H, R^5=H
4i: R^1=Br, R^2=H, R^3=H, R^4=H, R^5=H
4j: R^1=H, R^2=H, R^3=NO_2, R^4=H, R^5=H
4k: R^1=H, R^2=H, R^3=SCH_3, R^4=H, R^5=H
4l: R^1=H, R^2=NO_2, R^3=H, R^4=H, R^5=H
4m: R^1=H, R^2=Cl, R^3=H, R^4=H, R^5=H
4n: R^1=H, R^2=H, R^3=Cl, R^4=H, R^5=H
4o: R^1=H, R^2=Cl, R^3=Cl, R^4=H, R^5=H
4p: R^1=H, R^2=H, R^3=$COOCH_3$, R^4=H, R^5=H
4q: R^1=H, R^2=H, R^3=CN, R^4=H, R^5=H
4r: R^1=H, R^2=OCH_3, R^3=H, R^4=H, R^5=H
4s: R^1=H, R^2=H, R^3=CF_3, R^4=H, R^5=H
4t: R^1=H, R^2=H, R^3=OCH_3, R^4=H, R^5=H
4v: R^1=H, R^2=H, R^3=H, R^4=H, R^5=CH_3

Scheme 1. General approach for the synthesis of 9-*O*-substituted BBR derivatives **4a**-**4v**. Reaction conditions: i) 205 °C, 15 mbar, 2 h; ii) K_2CO_3 (5 eq.), anh. MeCN (or THF/MeCN (1:1) for **3b**), 80 °C, 1.5 h.

3.2 Cholinesterase inhibition

To determine the therapeutic potential of berberine derivatives (**4a**-**4v**) with particular emphasis for AD, their AChE and BChE inhibitory activities were assayed by the

modified spectrophotometric method described by Ellman *et al.* using human recombinant AChE (*h*AChE) and human serum BChE (*h*BChE), respectively [52]. Results are expressed as IC_{50} values and preference for *h*AChE is determined by the selectivity index (SI). These data are summarized in Table 1.

Table 1. *In vitro* results of BBR derivatives **4a**-**4v** and reference compound BBR

Compounds	POP IC_{50} ± SEM (μM)[a]	IC_{50} *h*AChE ± SEM (μM)[a]	IC_{50} *h*BChE ± SEM (μM)[a]	SI for *h*AChE (*h*BChE/*h*AChE)[b]
BBR	142 ± 21	17.4 ± 4.1	47.2 ± 3.3	2.7
4a	25.4 ± 2.8	5.0 ± 0.1	8.0 ± 0.4	1.6
4b	79.1 ± 8.7	7.3 ± 0.4	14.1 ± 0.8	1.9
4c	71.1 ± 7.9	10.4 ± 0.2	21.5 ± 1.3	2.1
4d	10.7 ± 1.2	75.8 ± 9.1	5.8 ± 0.2	0.08
4e	53.3 ± 6.1	4.2 ± 0.3	2.6 ± 0.1	0.6
4f	58.7 ± 8.4	2.5 ± 0.1	3.7 ± 0.1	1.5
4g	19.4 ± 4.4	3.3 ± 0.4	9.6 ± 0.4	2.9
4h	59.6 ± 5.5	2.7 ± 0.2	4.9 ± 0.1	1.8
4i	38.9 ± 4.9	1.7 ± 0.1	4.0 ± 0.1	2.3
4j	21.2 ± 3.0	0.99 ± 0.04	8.0 ± 0.2	8.1
4k	34.0 ± 2.5	2.6 ± 0.1	2.9 ± 0.1	1.1
4l	24.7 ± 1.3	1.45 ± 0.04	6.9 ± 0.2	4.8
4m	67.0 ± 3.0	1.9 ± 0.1	6.1 ± 0.3	3.2
4n	39.4 ± 1.4	2.5 ± 0.1	6.3 ± 0.2	2.5
4o	52.7 ± 2.2	1.22 ± 0.03	3.6 ± 0.1	3.0
4p	47.6 ± 1.4	2.6 ± 0.1	4.9 ± 0.1	1.9
4q	36.5 ± 3.0	1.7 ± 0.1	11.7 ± 0.3	6.8
4r	40.4 ± 1.0	3.5 ± 0.1	7.4 ± 0.1	2.1
4s	27.4 ± 1.3	1.3 ± 0.1	9.4 ± 0.2	7.0
4t	40.5 ± 0.9	5.3 ± 0.2	4.3 ± 0.1	0.8
4u	28.5 ± 1.7	1.5 ± 0.1	1.26 ± 0.02	0.8
4v	29.5 ± 1.3	0.79 ± 0.02	5.8 ± 0.1	7.3

[a] Results are expressed as the mean of at least three independent experiments; [b] Selectivity for *h*AChE is determined as ratio IC_{50}(*h*BChE)/IC_{50}(*h*AChE)

All the novel derivatives **4a**-**4v** displayed *h*AChE inhibition ability in micromolar to the sub-micromolar range. BBR, taken as a reference, displayed moderate inhibition ability with IC_{50} = 17.4 μM, which is roughly under other literature data [53]. The most active compound **4v** displayed high inhibitory potency with IC_{50} value 0.79 μM, which roughly corresponds to tacrine, formerly used for the AD treatment [54]. From the SAR analysis, it can be deduced that derivatives either unsubstituted or bearing methyl in a different positions (**4a**-**4d**) of

benzyl ring negatively affected the inhibition power decreasing the IC_{50} values from a single unit up-to two-digit micromolar concentration (IC_{50} = 5 - 76 µM). No other SAR can be drawn when taking into consideration either i) the position of substituents or ii) electron-donating/electron-withdrawing group characteristics. Comparing BBR derivates reported herein with simplified analogues containing core *N*-benzylphenethylamine moiety reported by Roselli *et al.*, almost identical IC_{50} values were found for AChE inhibition [55]. In the study by Huang *et al.* berberine derivates turned out to be more potent and more selective for AChE inhibition [56]. Nevertheless, the data cannot be compared because of the different origins of AChE and BChE species.

Since the levels of BChE are up-regulated in the advanced stages of AD, and BChE is also capable of compensating for the decreased activity of AChE, BChE emerged as a backup therapeutic option [14,57]. Accordingly, all the newly developed BBR derivatives **4a**-**4v** exerted BChE inhibition ability with IC_{50} values in the micromolar range (1.26 - 21.5 µM), all being more potent than parent BBR (IC_{50} = 47.2 µM). The top-ranked compound was **4u** (IC_{50} = 1.26 µM) having 37.5 times amplified potency compared to BBR. Similarly to AChE, no clear SAR could not be established given the nature of attached aromatic moiety.

In general, most of the BBR derivatives are *h*AChE selective inhibitors having SI values > 1.0 (Table 1). The highest SI score revealed 4-nitrophenyl derivative **4j** being 8.1 times more selective in inhibiting *h*AChE. On the contrary, **4d** revealed an intriguing *h*BChE selective profile with SI value for *h*BChE = 13.1.

3.3 Prolyl oligopeptidase inhibition

POP has been shown to participate in several aspects of the central nervous system (CNS) like learning, memory and mood, the features that are associated with AD [58]. It has been discussed that reduced POP activity correlated to the tau pathology and severity of the disorder [59]. Some of the POP inhibitors have been evaluated in clinical trials to reverse and/or attenuate memory loss [26]. It has been proposed that the extract of *Rhizoma coptidis* containing 23% of BBR as a major alkaloid was a potent POP inhibitor. The study also disclosed that IC_{50} value of isolated BBR was 145 ± 19 µM which is in accordance with our data (Table 1) [60]. All the novel BBR derivatives demonstrated IC_{50} values ranging from 10 to 79 µM corroborating that the 9-*O* aryl substitution is essential for activity increment. Analogue **4d** bearing 4-methylbenzyl appendage emerged as the most potent analogue from

the series (IC_{50} = 10.7 μM). From the obtained data, it can be roughly estimated that more active derivatives (IC_{50} < 30 μM) favor position 4- at attached benzyl moiety with electron-withdrawing groups like NO_2 or CF_3 (**4j** and **4s**, respectively), but also small electron-donating groups like methyl (**4d**) are well tolerated in this position.

3.4 Kinetic assay

Kinetic study was performed to describe the interactions of the compounds **4s** and **4u** with *h*AChE and *h*BChE. Inhibition kinetics was determined from velocity curves that were measured at several concentrations of tested compounds. The type of enzyme inhibition and corresponding kinetic parameters (K_i and $K_{i'}$) were determined using nonlinear regression analysis. Results for each type model of inhibition (competitive, non-competitive, uncompetitive and mixed) were compared by sum-of-squares F-test. Statistical analysis showed noncompetitive inhibition for **4s** with hAChE and mixed type of inhibition for **4u** with BChE ($p < 0.05$), which is in line with Lineweaver–Burk plot, used for better visualization of obtained data (Graph 1).

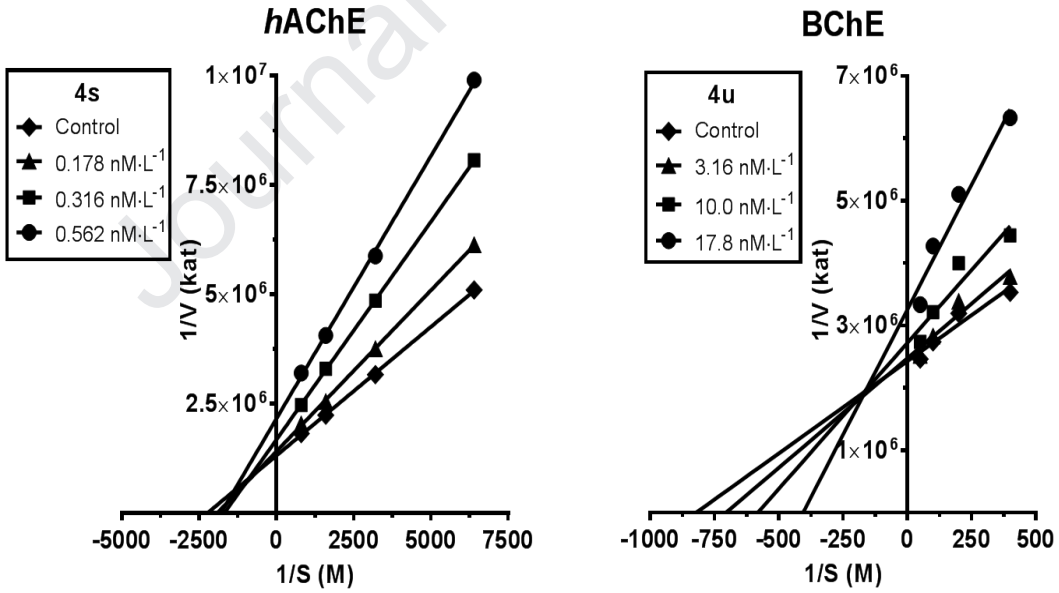

Graph 1. Steady state inhibition of cholinesterase substrate hydrolysis by compound **4s** (*h*AChE) and **4u** (BChE) at different concentrations. Lineweaver–Burk plots of initial velocity at increasing substrate concentrations (*h*AChE: 0.1563 - 1.250 mM; BChE: 2.5 - 20.0 mM) are presented. Lines were derived from a linear regression of the data points.

The intersection of lines is located on the x-axis for **4s** and above the axis for **4u**, which corresponds with reversible binding mode to both free enzyme and enzyme-substrate complex. Apparent V_{max} decreased with an increasing concentration of **4s** and K_m remained unchanged, indicating that it has an affinity for both the free *h*AChE and enzyme-substrate complex. Compound **4s** binds with higher affinity to the free BChE ($K_i < K_{i'}$), apparent V_{max} was reduced at higher concentration of inhibitor while the K_m was slightly increased. Both inhibitors interact with enzyme allosteric peripheral anionic site (PAS). This interaction causes conformational changes of the cholinesterase, yielding the change of its active site. A K_i value of 0.456 ± 0.041 nM was measured for **4s** on *h*AChE and a K_i value of 8.34 ± 1.99 nM and $K_{i'}$ of 75.6 ± 16.7 nM were determined for **4u** against BChE, respectively.

3.5 Molecular modeling studies

To further understand the activity enhancing effect of aryl attachment at 9-*O*-position of BBR core, we performed molecular modeling studies using X-ray structures of *h*AChE (PDB ID: 4EY6), *h*BChE (PDB ID: 4BDS) and human POP (PDB ID: 3DDU) [61–63]. All the proteins were downloaded in high resolution solved at 2.4 Å, 2.1 Å and 1.6 Å for AChE, BChE and POP, respectively.

Both enantiomers, namely *(R)*-**4v** and *(S)*-**4v**, were selected to elucidate which isomer presumably contribute more to activity increment, and both of them were also compared with reference BBR (Fig. 2). BBR spans the cavity gorge of AChE contacting esteratic site flanked by catalytic triad residues (His447, Ser203 and Glu202) forming hydrogen bond between hydroxyl Ser203 and oxygen from 1,3-dioxolane moiety (2.4 Å; Fig. 2 A, B). BBR also established T-shaped π-π interaction with Tyr337 (3.7 Å) and other hydrophobic contacts with Phe338 and Trp86 in the catalytic active site (CAS) of the enzyme. Quaternary nitrogen displayed salt bridge with carboxylic oxygen from Asp74. At the entrance of AChE, BBR is engaged in several hydrophobic interactions including π-π stacking with Phe297, and Tyr341, van der Waals contact with Trp286, and also hydrogen bond between hydroxyl from Tyr124 and 9-methoxy group from BBR (2.2 Å). *(S)*-**4v** (Fig. 2 E, F) revealed similar arrangement to BBR in the AChE active site; however, interaction with Ser203 is missing. Attachment of (*S*)-1-phenoxyethyl moiety yielded in π-alkyl contact with Tyr341, and π-π stacking with Trp286 and Tyr72. *(R)*-**4v** adopted close configuration like parent BBR (Fig. 2 C, D). Indeed, typical hydrogen bond between Ser203 and oxygen from 1,3-dioxolane moiety (2.8 Å), π-π contact

with Tyr337 (3.6 Å), favorable orientation between quaternary charge of BBR and Asp74 and other hydrophobic contacts in PAS region with Phe297, Tyr124, Phe338 and other amino acids, are all observed. Additionally, attachment of (*R*)-1-phenoxyethyl provided other favorable interaction like π-alkyl contact between methyl group and Tyr341, anion-π interaction with Asp74 and π-π displaced stacking with Tyr72 and Trp286. To conclude, missing interactions in *(S)*-**4v**-*h*AChE complex like hydrogen bond with Ser203 and also anion-π contact with Asp74 might be designated as the culprit for higher affinity of *(R)*-**4v** over *(S)*-**4v**, however, direct proof-of-concept from *in vitro* measurement is undoubtedly required to confirm the docking output.

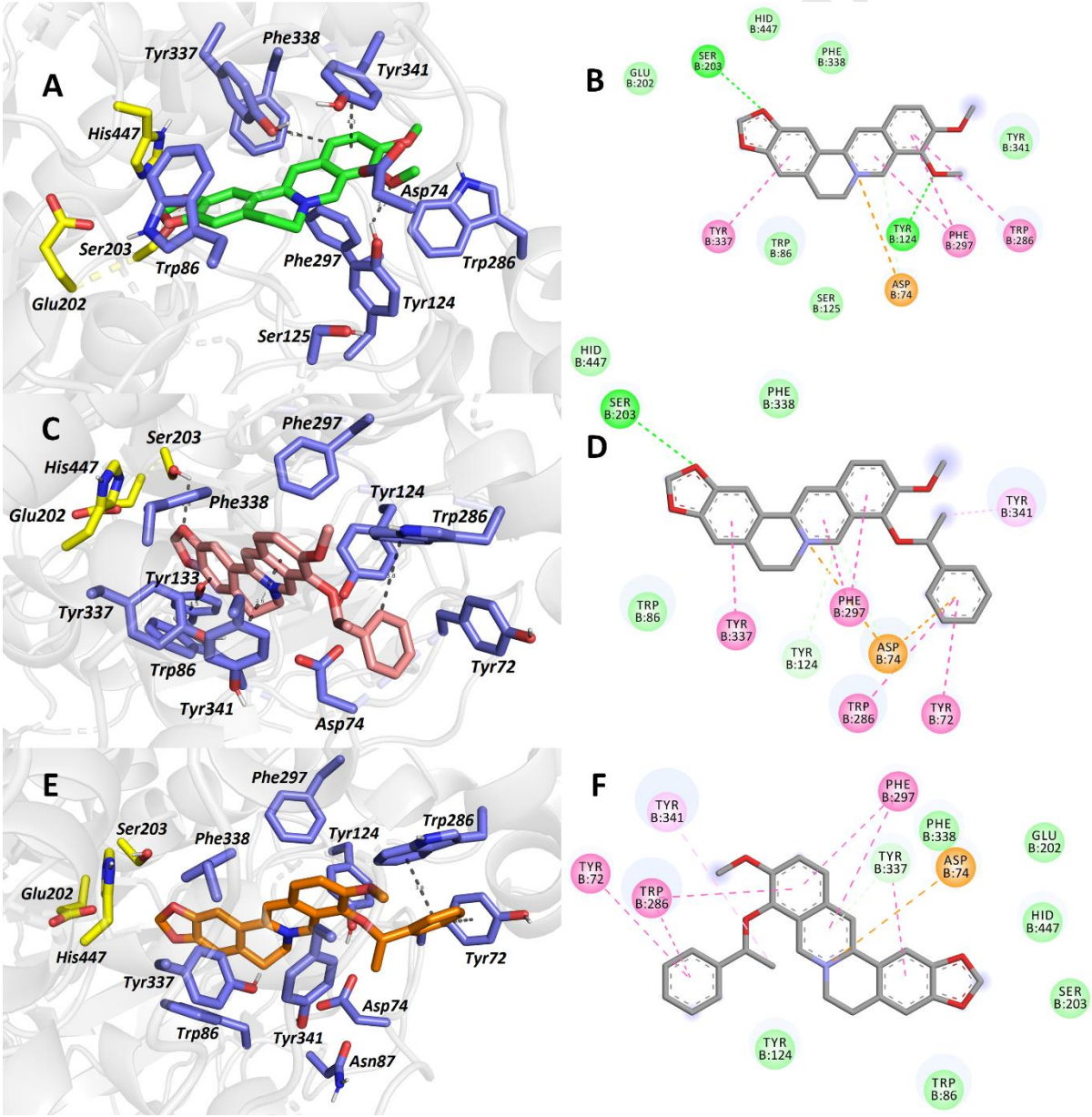

Figure 2. Docking of BBR (A, B), *(R)*-**4v** (C, D), *(S)*-**4v** (E, F) to the active site of *h*AChE (PDB ID: 4EY6) [61]. Generally to A, C, and E: BBR, *(R)*-**4v** and *(S)*-**4v** are shown in green, salmon and orange, respectively.

Important amino acid residues are highlighted in dark blue, catalytic triad residues in yellow. Apparent ligand-enzyme interactions are shown as dashed lines; distance is measured in Å. The rest of the enzyme is displayed as a grey transparent cartoon. Figures A, C and E were created with the PyMOL Molecular Graphics System, Version 2.0 Schrödinger, LLC. 2D figures (B, D, F) highlights the interaction of different nature between each ligand and specific amino acid residues. Figures B, D and F were generated by Discovery Studio 2016 Client software.

Top-ranked *h*BChE inhibitor **4u** and reference BBR were selected to inspect structural topology of these two ligands in *h*BChE active site (Fig. 3). BBR (Fig. 3 A, B) is settled in the vicinity of catalytic triad residues (Ser198, Glu197 and His438) displaying π-π interaction between His438 and ring *A* of BBR. Moreover, there is a strong π-π stacking with Trp82 from CAS and other aromatic regions of BBR. Other crucial interaction can be classified as either hydrogen bonding between methoxy oxygen and Gln119, or hydrophobic contacts with aliphatic amino acids like Asp70, Thr120, Ser198 and Ser287, as well as aromatic residue Phe329. It is well known, that BChE active site is larger in comparison with AChE and thus can accommodate bulkier substrates [64]. Bearing this in mind, such knowledge pave the way for **4u** bearing bulky (naphthalen-2-yl)methylene moiety. Indeed, **4u** revealed completely different pose to BBR in *h*BChE active site (Fig. 3 C, D). This accounts for parallel π-π stacking between Trp82 (3.8 - 4.0 Å) and (naphthalen-2-yl)methylene unit, engagement of Tyr332 by π-π interaction with *C* and *D* aromatic rings from BBR core, anion-π attractive forces with Asp70, and also hydrogen bond formation with hydroxyl group from Ser287. Thus, all these findings justify our design considerations and rationalize our findings from *in vitro*.

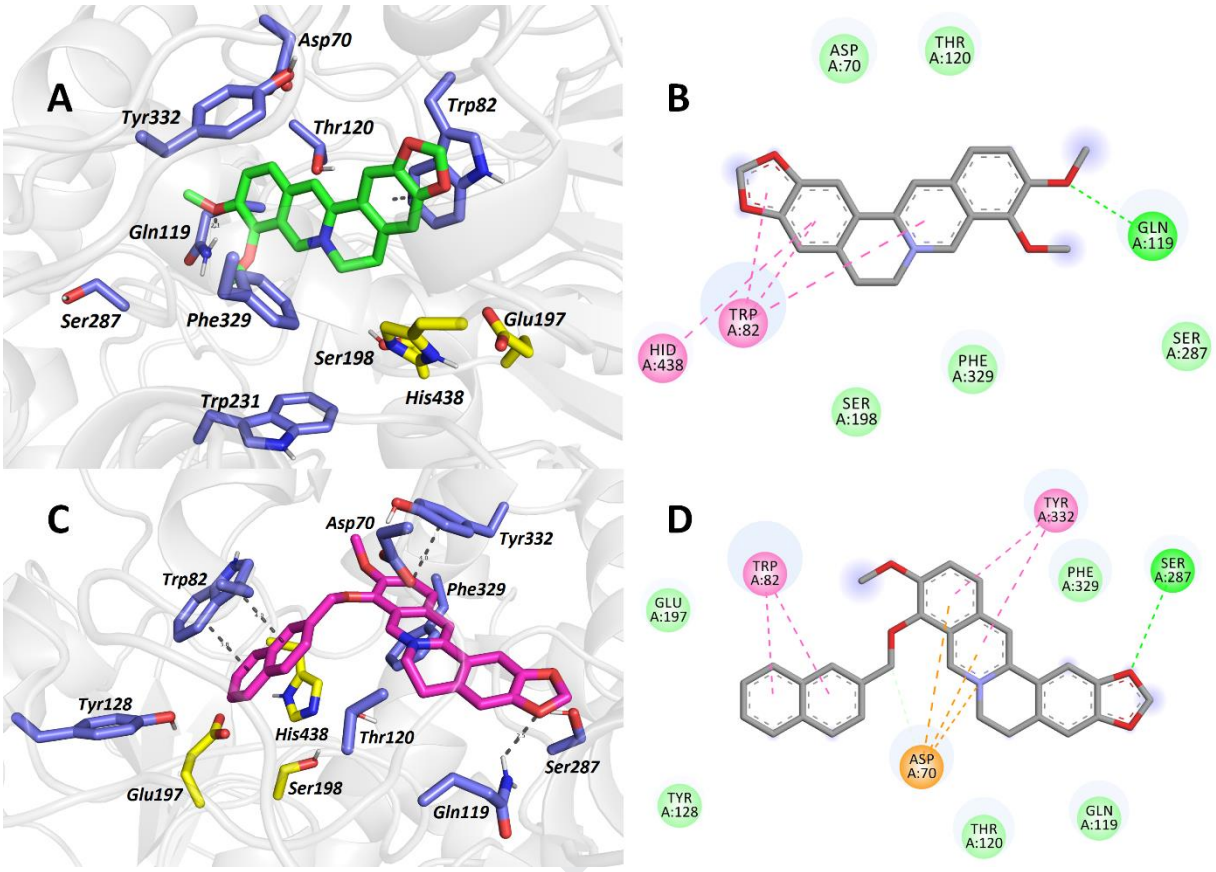

Figure 3. Docking of BBR (A, B) and **4u** to the active site of *h*BChE (PDB ID: 4BDS) [62]. Generally to A and C: BBR and **4u** are shown in green and purple, respectively. Important amino acid residues are highlighted in dark blue, catalytic triad residues in yellow. Apparent ligand-enzyme interactions are shown as dashed lines, distance is measured in Å. The rest of the enzyme is displayed as grey transparent cartoon. Figures A and C were created with the PyMOL Molecular Graphics System, Version 2.0 Schrödinger, LLC. 2D figures (B and D) highlights the interaction of different nature between each ligand and specific amino acid residues. Figures B and D were generated by Discovery Studio 2016 Client software.

BBR and **4d** as the highlighted POP inhibitor were further subjected to molecular docking studies to reveal their arrangement in POP active site (Fig. 4). The active site of human POP, defined by a catalytic triad, is composed of the amino acid residues Ser554, His680 and Asp641, and is located at the interface of the two domains in the cavity gorge [65]. The active site may be further divided into three regions, named as S1, S2 and S3. The S1 site of the protein is narrow and can accommodate proline like moieties and the nucleophilic appendages attached to proline like rings. This substitution is known to enhance the activity of inhibitors because it enables interaction with Ser554. The S2 site with Asp641 favors positive charge whereas the third site S3 is flanked with amino acids like Phe173, Met235, Cys255, Ile591, and Ala594 therefore hydrophobic groups as a part of bulky ligands can be lodged there [66]. BBR (Fig. 4 A, B) is located in the vicinity of catalytic triad displaying

π-π contact with His680 and van der Waals attractive forces with Ser554. Ring *A* is implicated in the classical π-π stacking with Phe476 (4.8 Å) and Trp595 (4.3 Å). Cys255 play an important role in ligand placement by showing π-sulfur and π-alkyl interactions with *C* and *D* rings, respectively. 10-Methoxy moiety is anchored by hydrogen bonds to Arg252 (2.1 and 2.3 Å). The most remarkable finding is that positively charged nitrogen of BBR exerted unfavorable positive-positive interaction with Arg643 which is presumably responsible for its relatively low inhibitory potency observed *in vitro*. On the contrary, **4d** is placed outside the catalytic triad contacting only Ser554 by van der Waals forces (Fig. 4 C, D). 4-Methylbenzyl attachment revealed several hydrophobic contacts to Cys255, Trp595 and Phe476. Interestingly, another Arg residue, namely Arg643 displayed hydrogen bond with 10-methoxy group. This trend was also observed for BBR (Fig. 4 A, B) with Arg252. Phe173 can be highlighted as the key-mediator residue in **4d**-POP complex orchestrating the topology of BBR core scaffold by anchoring it to *A*, *C* and *D* aromatic regions. Notably, unfavorable interaction between **4d** and Arg643 is missing. Taken also into account all the aforementioned, these interactions can be mostly responsible for high POP potency of **4d**.

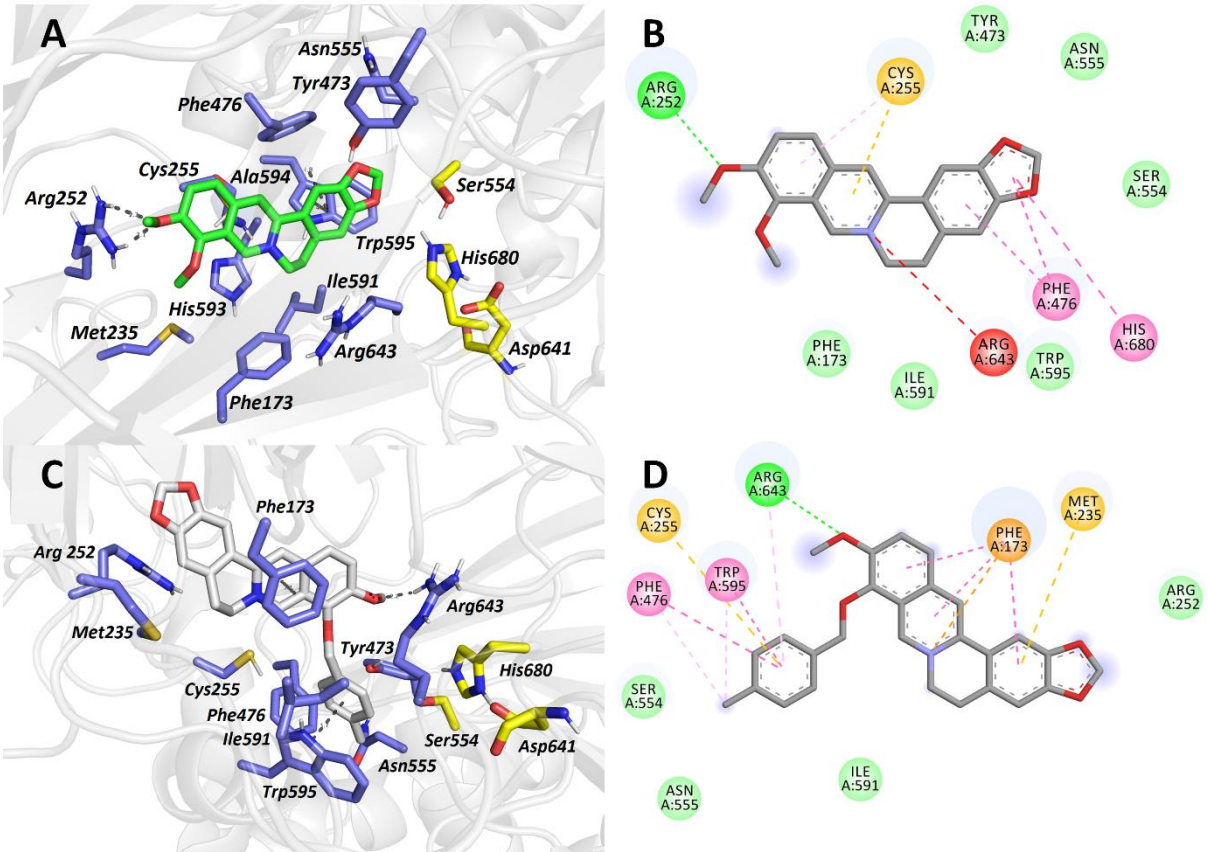

Figure 4. Docking of BBR (A, B) and **4d** to the active site of human POP (PDB ID: 3DDU) [63]. Generally to A and C: BBR and **4d** are shown in green and grey, respectively. Important amino acid residues are

highlighted in dark blue, catalytic triad residues in yellow. Apparent ligand-enzyme interactions are shown as dashed lines, distance is measured in Å. The rest of the enzyme is displayed as grey transparent cartoon. Figures A and C were created with the PyMOL Molecular Graphics System, Version 2.0 Schrödinger, LLC. 2D figures (B and D) highlights the interaction of different nature between each ligand and specific amino acid residues. Figures B and D were generated by Discovery Studio 2016 Client software.

3.6 Quantitative structure-activity relationship (QSAR) analyses

QSAR analyses were performed on PM3 geometrically optimized structures of **4a - 4v** in Schrodinger 2020-1 employing its tools for chemoinformatics and machine learning. The first investigated, deep chemistry convolutional neural network QSAR modeling (DC-CNN QSAR) based on processing molecular graphs by TensorFlow/Keras libraries, unfortunately, provided no statistically significant SAR when the input dataset of 22 compounds was randomly split into training and test sets in 75:25 ratio. The low predictivity of DC-CNN QSAR models, in terms of negative cross-validated coefficients of determination Q^2 for the prediction in the test set, was mainly caused by the insufficient size of the dataset. No significant improvement was achieved by the Atom-based QSAR analyses. Better results were achieved by the AutoQSAR function, which applied a kernel partial least regression (kPLS) on a set of various molecular descriptors utilizing an algorithm for selecting optimal molecular descriptor subsets. As in the kPLS all the input variables are projected in reproducing kernel Hilbert space by a Gaussian transform (Eq. 1), kPLS is able to recognize nonlinear features in the data.

$$K_{i,j} = e^{-\frac{d_{ij}^2}{\sigma_{ij}^2}} \qquad \text{(Equation 1)}$$

The kernel function $K_{i,j}$ replaces the scalar products of X matrix of molecular descriptors in the PLS algorithm, taking d_{ij} argument as Euclidian distance between descriptors *i* and *j.* The nonlinearity of the kernel is additionally modulated by the parameter σ_{ij}.

The AutoQSAR program automatically tested hundreds of models and various setting and selected the best scoring ones. In the final kPLS QSAR models, only one latent factor was used. The best statistical kPLS QSAR models for the values of log IC_{50} (POP), log IC_{50} (*h*AChE), and log IC_{50} (*h*BChE) are briefly described in Table 2.

Table 2. Statistical overview of kPLS QSAR models found for the studied compounds.

Target	$R^{2\,a}$	S.D. [b]	RMSE [c]	$Q^{2\,d}$	Q^2(MW) [e]
POP	0.7160	0.1170	0.1015	0.7425	-0.0387
*h*AChE	0.8460	0.1841	0.1053	0.8801	0.5204
*h*BChE	0.7738	0.1390	0.1358	0.5440	0.3535

[a] Coefficient of determination for the training set (training and test samples were divided randomly in 75:25 ratio); [b] standard deviation of prediction for the training set; [c] root-mean-square error for the test set prediction; [d] coefficient of determination for the test set prediction; [e] coefficient of determination for the test set prediction if only molecular weight is used as a predictor (the above statistical criteria definitions were adopted from the Schrödinger manual).

According to the statistical criteria given in Table 2, all three QSAR models are statistically significant and can be used for representing the biological properties of the studied compounds. Thanks to the incorporation of fingerprints in the matrix of molecular descriptors, the most influencing atoms in the structures can be determined by pseudo-beta coefficient analysis. Structural features that likely improve or deteriorate the biological activity of the studied targets are outlined in Fig. 5.

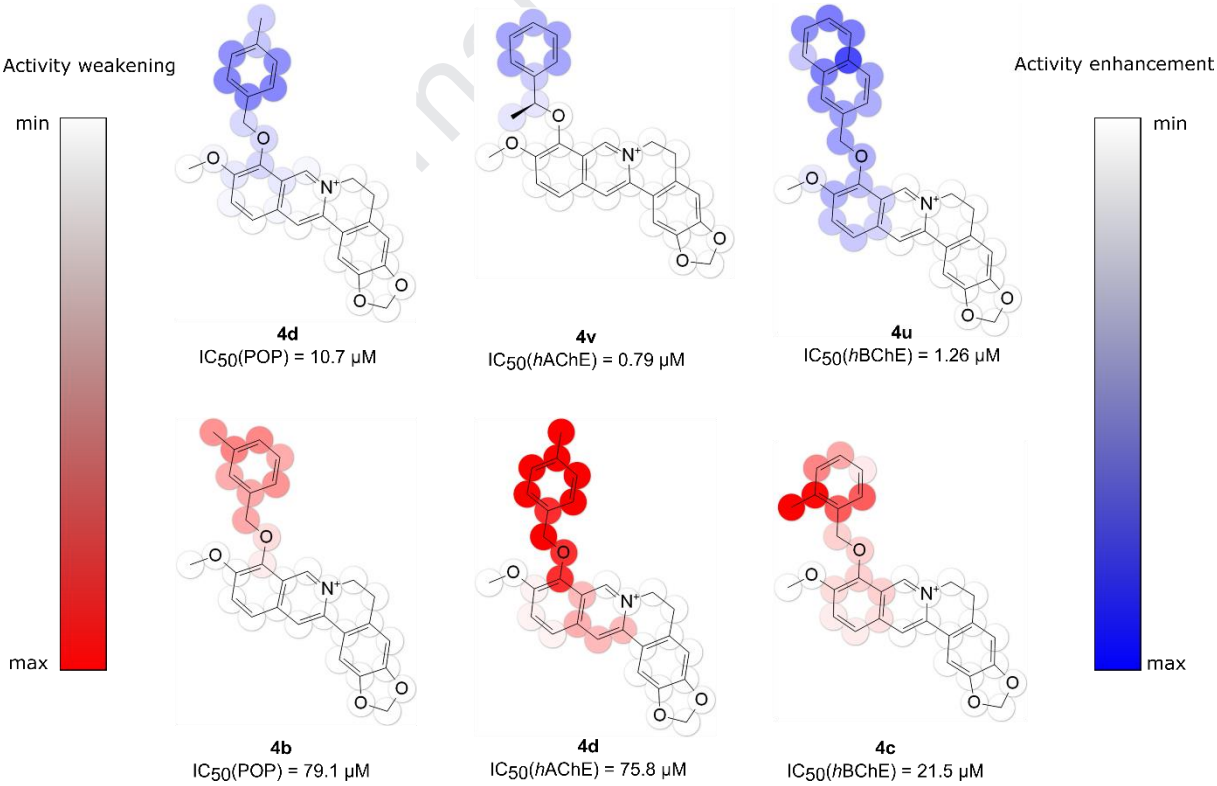

Figure 5. Analysis of kPLS QSAR models with respect to molecular fingerprint contributions. Molecular features with a positive effect on IC_{50} are colored in blue, features with a detrimental impact on IC_{50} (e.g. lowering its value) are colored in red shadows.

From the analysis of fingerprint contributions in kPLS QSAR models (Fig. 5), it is obvious that there are only subtle structural differences controlling whether a substructure weakens or enhances the biological activity. For instance, the change of methyl group position from *para* to *meta* switches the impact of the methylbenzyloxy function on the biological activity against *h*AChE dramatically. Noteworthy, the same structural feature that weakens the biological activity against *h*AChE (**4d**) induces substantial enhancement of the biological activity against POP. More details on fingerprint contributions can be found in Supplementary Information (S2-S4). In general, it would be very challenging to intuitively design improved inhibitors of POP and *h*AChE/*h*BChE in such variable structure-activity space, but the developed kPLS QSAR models could serve in this case to predict the biological activity by ligand-based virtual screening with satisfying ability.

3.7 Cytotoxicity

The effect on cell proliferation of BBR derivatives using the Chinese hamster ovary cell line (CHO-K1) is presented in Table 3 [67]. MTT (3-[4,5-dimethylthiazol-2-yl]-2,5 diphenyl tetrazolium bromide) assay was applied to reveal the cytotoxic effect [68]. It is evident that aryl substitution of BBR scaffold at 9-*O*- noticeably affected cytotoxicity resulting in higher toxic species. This trend nicely correlates with lipophilicity increment defined by calculated logP values (Table 3). Accordingly, **4o** as the most lipophilic BBR derivative containing 3,4-dichlorobenzyl moiety is the most toxic species from the subset. The position of each specific substituent does not play any significant role, i.e. no cytotoxicity differences were observed within small subsets like **4b**-**4d** (methyl substitution), **4g-4i** (bromine attachment), and **4r** with **4t** (methoxy derivatives). Unsubstituted derivative (**4a**), or analogues containing methyl (**4b**-**4d**) or polar groups (**4p**, methyl ester; **4q**, cyano group) displayed higher cell viability, i.e. lower cytotoxicity profile. Derivative **4q** was the least toxic in the family of newly developed BBR with IC_{50} value lying in the same range as BBR.

Table 3. Cytotoxic potential of BBR and novel derivatives **4a**-**4v** determined using CHO-K1 cell lines.

Compounds	CHO-K1 cell line MTT IC_{50} ± SEM (μM) [a]	clogP [c]
berberine	336 ± 87	-1.28
4a	55 ± 19	0.44
4b	58 ± 1	0.95
4c	55 ± 8	0.95
4d	43 ± 5	0.95
4e	17 ± 3	1.69

4f	23 ± 1	1.47
4g	48 ± 9	1.21
4h	32 ± 8	1.21
4i	26 ± 7	1.21
4j	n.d. [b]	0.38
4k	43 ± 6	1.07
4l	30 ± 6	0.38
4m	30 ± 2	1.05
4n	13 ± 1	1.05
4o	9 ± 2	1.65
4p	50 ± 6	0.44
4q	292 ± 37	0.30
4r	46 ± 1	0.28
4s	21 ± 4	1.32
4t	42 ± 3	0.28
4u	14 ± 2	1.43
4v	42 ± 4	0.86

[a] Results are expressed as the mean of at least three experiments; [b] Not determined; low solubility profile; [c] calculated partition coefficient (clogP) between *n*-octanol and water using MarvinSketch software v. 17.17.0

3.8 In vitro antioxidant properties

To investigate the radical scavenging properties of berberine derivatives (**4a-4v**) 1,1-diphenyl-2-picryl-hydrazyl (DPPH) assay was used (Table 4) [69]. The EC_{50} values of standards of trolox, *N*-acetylcysteine, and BBR were compared with published results [70–73]. Demethylation in position 9- yielding to berberrubine (**2**) with free phenolic group enabled a remarkable increase in antioxidant activity (EC_{50} = 87 ± 6.7 μM) [70]. For the novel derivatives, only compounds **4a-4f** possessed higher antioxidant capacity compared to BBR with top-ranked derivative **4f** (EC_{50} = 990 μM). It can be deduced that slight activity improvement is associated with small aliphatic substituents (mostly methyl groups), not depending on their exact position within the attached aryl moiety. These results are, however, still far from the concentration scale found for trolox or *N*-acetylcysteine (EC_{50} = 16 and 28 μM, respectively). Antioxidant activity of novel BBR derivatives can thus be regarded as improbable.

Table 4. Antioxidant properties of reference compounds (Trolox and *N*-acetylcysteine), BBR and novel derivatives **4a**-**4v** established by DPPH assay.

Compounds	DPPH assay EC_{50} ± SEM (μM) [a]
4a	1,900 ± 80
4b	1,200 ± 35
4c	1,200 ± 50

4d	1,900 ± 47
4e	1,300 ± 110
4f	990 ± 31
4g	> 6,000
4h	2,200 ± 260
4i	> 6,000
4j	5,000 ± 390
4k	> 6,000
4l	5,600 ± 280
4m	5,400 ± 270
4n	5,200 ± 180
4o	> 6,000
4p	5,300 ± 250
4q	> 6,000
4r	5,300 ± 270
4s	5,300 ± 210
4t	> 6,000
4u	> 6,000
4v	5,600 ± 200
berberine	5,500 ± 310
trolox	16.2 ± 0.4
N-acetylcysteine	27.9 ± 1.8

[a] Results are expressed as the mean of at least three experiments

3.9 Inhibition of amyloid-β aggregation

Aβ is an intrinsically disordered protein forming insoluble extracellular deposits [74,75]. Accumulation of amyloid fibrils and their association with other macromolecules generate amyloid plaques [4]. Aβ overproduction and its decreased clearance are responsible for neuroinflammation response, neurodegeneration due to oxidative processes, disbalance in ion homeostasis, all leading to neuronal dysfunction and death [76]. Since BBR is capable to reduce levels of Aβ [34,77], we determined anti-amyloid profile of the most perspective berberine derivatives **4d**, **4u** and **4v**. Doxycycline was selected as a reference compound known for anti-amyloidogenic property [78]. At 50 μm concentration, all the tested derivatives revealed high $A\beta_{1-42}$ inhibition activity compared to BBR, ranging between 82 to 97% (Table 5). The most efficient one was derivative **4u**.

Table 5. Inhibition of $A\beta_{1-42}$ aggregation by the tested compounds at 50 μM concentration.

Compound	Inhibition of $A\beta_{1-42}$ aggregates ±SEM (%) [a]
BBR	70.5 ± 6.0
4d	82.6 ± 1.2
4u	97.2 ± 3.4

4v	86.7 ± 4.5
doxycycline	~ 100

[a] Inhibition ability of the compound to block $A\beta_{1-42}$ was measured in 1:1 ratio (compound: $A\beta_{1-42}$) at 50 μM. The results are the mean of three independent measurements each performed in duplicates.

3.10 Inhibition of tau protein self-aggregation

Tau (τ) tau phosphorylation is considered to be a major player in pathogenesis of AD. Abnormally hyperphosphorylated τ generates neurofibrillary tangles, which contain paired helical filaments [79]. A wealth of evidence proved that τ lesions correlate well with the severity of dementia [80]. BBR is known to experimentally ameliorate hyperphosphorylation of τ, and reducing cognitive impairment simultaneously [35]. Building on that fact, **4d**, **4u** and **4v** were selected as possible inhibitors of $\tau_{306-336}$ peptide aggregation. Results from Table 6 demonstrate that all the compounds are potent inhibitors of τ aggregation ranging from 31.9 to 62.0%. **4u** yielded the best even surpassing reference compound doxycycline (39.6%) inhibitory activity (Fig. 6).

Table 6. Inhibition activity of novel berberine derivatives **4d**, **4u** and **4v** on τ self-aggregation. BBR and doxycycline were used as positive references.

Compound	Inhibition of $\tau_{306-336}$ peptide self-aggregation ± SEM (%)[a]
BBR	25.0 ± 4.6
4d	31.9 ± 3.6
4u	62.0 ± 4.9
4v	38.3 ± 2.4
doxycycline	39.6 ± 0.5

[a] Inhibition of $\tau_{306-336}$ self-aggregation was measured in 1:1 ratio (compound:$\tau_{306-336}$) at 25 μM. The results are the mean of at three independent measurements each performed in duplicates.

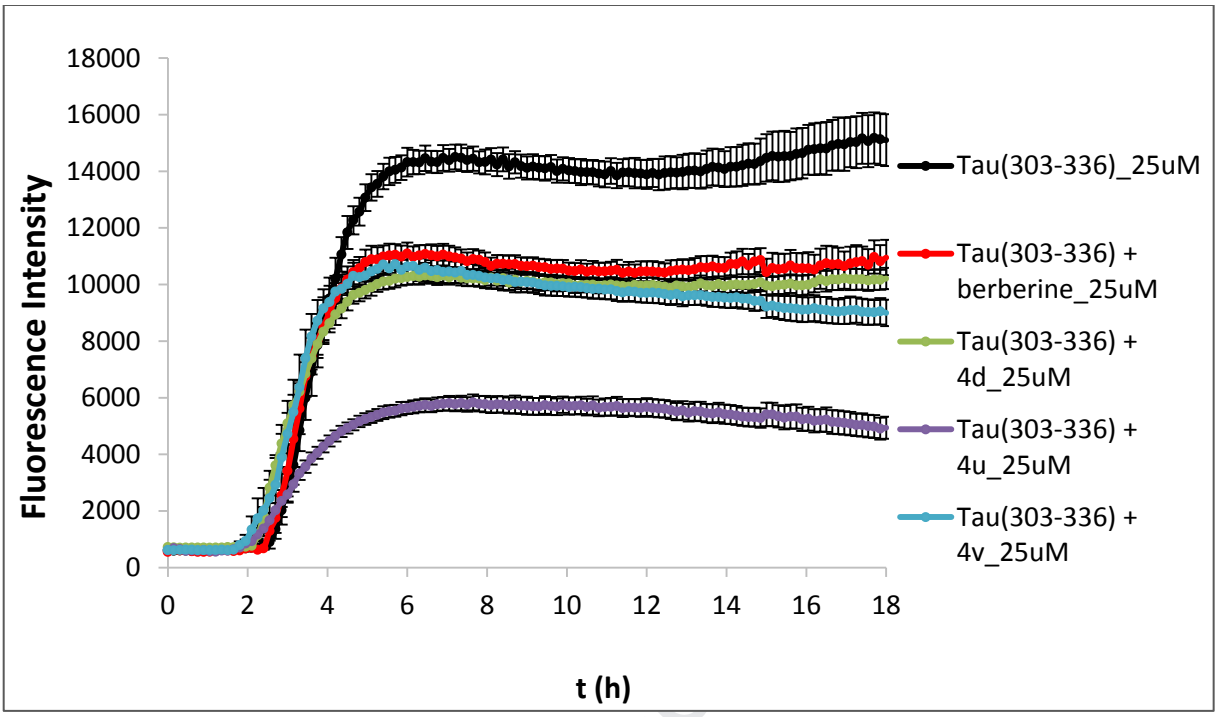

Figure 6. Thioflavin (ThT) was selected as fluorescent dye to visualize inhibitory activity of novel BBR derivatives, BBR and doxycycline as reference compound.

3.11 In vitro blood-brain barrier permeation

Penetration across the blood-brain barrier (BBB) is an essential property for compounds targeting the CNS. To predict BBB penetration of chosen BBR derivatives, parallel artificial membrane permeation assay (PAMPA) was applied (Table 7) [81,82]. For the estimation of prediction of BBB penetration via passive diffusion, we have selected analogues with balanced POP and ChE inhibition properties, i.e. **4a**, **4g**, **4j**, **4l**, and **4s** and **4u** as non-selective ChE inhibitor with highest BChE inhibition profile, top-ranked POP inhibitor **4d**, and also the most potent AChE inhibitor **4v**. We also measured other drugs serving either as positive or negative controls, for which CNS availability is known and also reported using the PAMPA assay (Table 7) [81,82]. According to our methodology using porcine lipid bilayer only the analogue **4t** was predicted to be capable of entering the brain via passive diffusion. The other analogues, as well as BBR, failed to show such properties. Such findings can be explained by the presence of permanently charged nitrogen impeding hydrophobic interactions between BBR analogues with the barrier yielding no or very low permeability by passive diffusion. Results obtain herein should be taken with precaution since some other studies displayed that BBR itself is the centrally active drug that can accumulate in hippocampus to provide a neuroprotective effect after intravenous administration in rat

[83]. Since PAMPA is considered as a powerful screening tool in early drug discovery, it is however hampered by several limitations i) not taking into account the phospholipid bilayer difference (porcine vs. human), ii) omitting active transport systems, and iii) excluding paracellular transport route which is typical for some small hydrophobic compounds [84].

Table 7. Estimation of BBB permeation of BBR, its derivatives and reference compounds

Compound	*Pe* ± SEM (*10^{-6} cm s^{-1})[a]	Prediction of BBB penetration[b]
BBR	0.2 ± 0.02	CNS –
4a	0.4 ± 0.06	CNS –
4d	0.8 ± 0.06	CNS –
4g	0.6 ± 0.2	CNS –
4j	1.4 ± 0.4	CNS –
4l	1.2 ± 0.04	CNS –
4s	0.8 ± 0.04	CNS –
4t	4.8 ± 1.4	CNS +
4u	0.8 ± 0.4	CNS –
4v	0.4 ± 0.1	CNS –
cefuroxime	0.3 ± 0.09	CNS –
furosemide	0.1 ± 0.003	CNS –
piroxicam	2.5 ± 0.4	CNS +/–
donepezil	9.8 ± 0.4	CNS +
rivastigmine	12.6 ± 3.0	CNS +
tacrine	6.0 ± 0.6	CNS +

[a] Results are expressed as the mean of at least three experiments; [b] CNS +: high BBB permeation predicted with *Pe* (10^{-6} cm.s^{-1}) > 4.0, CNS -: low BBB permeation predicted with *Pe* (10^{-6} cm.s^{-1}) < 2.0, CNS +/-: BBB permeation uncertain with *Pe* (10^{-6} cm.s^{-1}) from 4.0 to 2.0.

4 CONCLUSION

Phytochemicals represent an indispensable source in drug discovery serving as useful templates. This is especially important when pursuing neurodegenerative disorders like AD. BBR is one such successful example of alkaloid with a very low toxicity profile that has been validated in 77 clinical trials in different areas so far [85]. Being inspired by the success of BBR itself, we inspected the pharmacological profile of 22 novel BBR derivatives being both ChE and POP inhibitors. When designing multi-target drugs, the current challenge is to implement the same degree of modulation for each target [86]. Generally, almost all the

compounds were more profound inhibitors compared to parent BBR. Achieving a balanced activity towards the aforementioned targets is somehow coined to the structures of **4a**, **4g**, **4j**, **4l,** and **4s**, all being one-to-two digit micromolar inhibitors of the respective enzymes. For the specific targets, **4d**, **4v,** and **4u** can be highlighted as the most pronounced POP, AChE and BChE inhibitors, respectively. Molecular modeling studies between selected ligands and POP, AChE and BChE, respectively, revealed determinants responsible for the improved biological profile compared to BBR and justified 9-*O* aryl substitution. Data for the cytotoxicity clearly correlated well with the overall lipophilicity increment of each substituent with derivatives bearing polar groups like cyano (**4q**) being the least toxic. The antioxidant profile is presumably associated with the presence of a free phenolic group like in berberrubine (**2**). Having said that, novel compounds reported herein revealed only marginal antioxidant properties, which may be regarded as improbable at physiological conditions. We also discussed the central availability of BBR derivatives in PAMPA assay where one derivative (**4t**) displayed a possibility to be transported into the brain by passive diffusion. However, direct proof-of-concept by performing *in vivo* animal studies is undoubtedly required given the fact that BBR itself that failed in our test, is known to act centrally. Encouraging results of **4d**, **4u** and **4v** as possible cognitive enhancers prompted us to validate their disease-modifying properties. All three derivatives showed remarkable results highlighting **4u**. Consistently, **4u** outperformed BBR and acted similarly or even better compared to doxycycline when challenged to $A\beta_{1\text{-}42}$ and $\tau_{306\text{-}336}$. To conclude, we believe that this study may broaden the current knowledge in the development of novel multi-potent therapeutics derived from BBR with potential implications in neurodegenerative disorders like AD.

5 EXPERIMENTAL SECTION

5.1 General Chemical Methods

All of the chemical reagents used were purchased from Sigma-Aldrich (Czech Republic). Solvents for synthesis were obtained from Penta Chemicals Co (Czech Republic). The course of the reactions was monitored by thin-layer chromatography (TLC) on aluminum plates pre-coated with silica gel 60 F_{254} (Merck, Czech Republic) and then visualized by UV at 254 nm wavelength. Melting points were determined on a microheating stage PHMK 05 (VEB Kombinant Nagema, Radebeul, Germany) and are uncorrected. Uncalibrated purity was ascertained by LC−UV using a reverse phase C18 chromatographic column. All of the

biologically tested compounds exhibited purity 96−99% at a wavelength 254 nm. NMR spectra of target compounds were recorded on a Varian Mercury VX BB 300 (operating at 300 MHz for ^{1}H and 75 MHz for ^{13}C) or on a Varian S500 spectrometer (operating at 500 MHz for ^{1}H and 126 MHz for ^{13}C; Varian Comp. Palo Alto, CA). Chemical shifts are reported in parts per million (ppm). Spin multiplicities are given as s (singlet), bs (broad singlet), d (doublet), dd (doublet of doublets), t (triplet), q (quartet), or m (multiplet). The coupling constants (*J*) are reported in hertz (Hz). All the ^{1}H and ^{13}C NMR spectra are listed in Supplementary Information. High-resolution mass spectra (HRMS) were determined by a Q Exactive Plus hybrid quadrupole-orbitrap spectrometer.

5.1.1 Synthesis of berberrubine

The synthesis of berberrubine was carried out according to literature method [87]. Berberine chloride (5 g, 0.01 M) was placed into the round bottom flask and heated at 205 °C in a vacuum under reduced pressure (15 mbar) for 2 hours turning yellow BBR to dark red berberrubine with no need of further purification. Spectral data were in agreement with literature [45].

5.1.2 General procedure for the synthesis of 9-*O*-aryl-berberine bromides (4a-4v)

Berberrubine (0.5 g, 1.4 mM) and potassium carbonate (0.97 g, 2.1 mM) were treated with anhydrous MeCN (30 mL) at 80 °C for 30 min. Subsequently, the appropriate rate of arylmethylene bromide (1.5eq) was added. The reaction mixture was refluxed at 80 °C for 1h. After filtration and washing with MeCN (50 mL) and MeOH (50 mL), solid residues were purified via column chromatography was used for purification using CH_3Cl/MeOH (5:1, v/v) as eluent. Reagent **3b** had to be dissolved in 15 mL THF first because of its low solubility in MeCN following the aforementioned synthetic pathway.

5.1.2.1 9-*O*-benzylberberine bromide (4a)

Yield 34%; mp 181-184 °C; ^{1}H NMR (300 MHz, DMSO-d_6): δ 9.74 (s, 1H), 8.93 (s, 1H), 8.19 (d, *J* = 9.1 Hz, 1H), 7.99 (d, *J* = 9.1 Hz, 1H), 7.76 (s, 1H), 7.63 – 7.56 (m, 2H), 7.45 – 7.38 (m, 1H), 7.38 – 7.31 (m, 2H), 7.07 (s, 1H), 6.16 (s, 2H), 5.35 (s, 2H), 4.92 (t, *J* = 6.3 Hz, 2H), 4.07 (s, 3H), 3.18 (t, *J* = 6.3 Hz, 2H). ^{13}C NMR (75 MHz, DMSO-d_6): δ 150.9, 150.0, 147.9, 145.5, 142.1, 137.6, 136.6, 133.1, 130.8, 129.0, 128.6, 128.5, 126.7, 123.9, 122.0, 120.6, 120.4, 108.6, 105.6, 102.3, 75.5, 57.2, 55.5, 26.5. HRMS $[M+H]^+$: 412.1542 (calculated for: $[C_{26}H_{22}NO_4]^+$ 412.1543)

5.1.2.2 9-*O*-(3-methylbenzyl)berberine bromide (4b)

Yield 46%; >300 °C decomposition; ^{1}H NMR (500 MHz, DMSO-d_6): δ 9.74 (s, 1H), 9.00 (s, 1H), 8.20 (d, J = 8.9 Hz, 1H), 8.03 (d, J = 8.9 Hz, 1H), 7.79 (s, 1H), 7.43 (s, 1H), 7.35 (d, J = 7.5 Hz, 1H), 7.25 (t, J = 7.5 Hz, 1H), 7.14 (d, J = 7.5 Hz, 1H), 7.07 (s, 1H), 6.15 (s, 2H), 5.29 (s, 2H), 4.92 (t, J = 6.4 Hz, 2H), 4.07 (s, 3H), 3.18 (t, J = 6.4 Hz, 2H), 2.31 (s, 3H). ^{13}C NMR (126 MHz, DMSO-d_6): δ 150.9, 149.9, 147.8, 145.5, 142.2, 137.7, 137.4, 136.5, 133.1, 130.8, 129.6, 129.1, 128.4, 126.7, 126.1, 124.0, 122.0, 120.6, 120.4, 108.6, 105.7, 102.2, 75.6, 57.3, 55.5, 26.5, 21.1. HRMS $[M+H]^+$: 426.1697 (calculated for: $[C_{27}H_{24}NO_4]^+$ 426.1700)

5.1.2.3 9-*O*-(2-methylbenzyl)berberine bromide (4c)

Yield 48%; mp 199-202 °C; ^{1}H NMR (300 MHz, DMSO-d_6): δ 9.59 (s, 1H), 9.03 – 9.01 (m, 1H), 8.22 (d, J = 8.9 Hz, 1H), 8.06 (d, J = 8.9 Hz, 1H), 7.80 (s, 1H), 7.58 (d, J = 7.1 Hz, 1H), 7.26 – 7.18 (m, 3H), 7.07 (s, 1H), 6.15 (s, 2H), 5.34 (s, 2H), 4.88 (m, 2H), 4.04 (s, 3H), 3.18 – 3.14 (m, 2H), 2.43 (t, 3H). ^{13}C NMR (75 MHz, DMSO-d_6): δ 151.1, 150.0, 147.8, 145.4, 142.4, 137.5, 137.0, 134.9, 133.2, 130.8, 130.3, 129.7, 128.6, 126.7, 126.0, 124.1, 121.9, 120.6, 120.5, 108.6, 105.7, 102.3, 73.7, 57.2, 55.7, 26.5, 18.8. HRMS $[M+H]^+$: 426.1697 (calculated for: $[C_{27}H_{24}NO_4]^+$ 426.1700)

5.1.2.4 9-*O*-(4-methylbenzyl)berberine bromide (4d)

Yield 86%; mp 216-218 °C; ^{1}H NMR (500 MHz, DMSO-d_6): δ 9.71 (s, 1H), 8.95 (s, 1H), 8.18 (d, J = 9.1 Hz, 1H), 7.99 (d, J = 9.1 Hz, 1H), 7.77 (s, 1H), 7.46 (d, J = 7.5 Hz, 2H), 7.18 (d, J = 7.5 Hz, 2H), 7.07 (s, 1H), 6.15 (s, 2H), 5.30 (s, 2H), 4.91 (t, J = 6.4 Hz, 2H), 4.06 (d, J = 8.7 Hz, 3H), 3.18 (t, J = 6.4 Hz, 2H), 2.28 (s, 3H); ^{13}C NMR (126 MHz, DMSO-d_6): δ 150.9, 150.0, 147.8, 145.5, 142.2, 137.9, 137.5, 133.6, 133.1, 130.8, 129.2, 129.0, 126.7, 123.8, 122.0, 120.6, 120.4, 108.6, 105.6, 102.2, 75.4, 57.2, 55.5, 26.5, 21.0. HRMS $[M+H]^+$: 426.1697 (calculated for: $[C_{27}H_{24}NO_4]^+$ 426.1700)

5.1.2.5 9-*O*-(4-isopropylbenzyl)berberine bromide (4e)

Yield 65%; mp 207-209 °C; ^{1}H NMR (500 MHz, DMSO-d_6): δ 9.70 (s, 1H), 8.93 (s, 1H), 8.20 (d, J = 9.1 Hz, 1H), 8.00 (d, J = 9.0 Hz, 1H), 7.78 (s, 1H), 7.49 (d, J = 7.7 Hz, 2H), 7.26 (d, J = 7.7 Hz, 2H), 7.08 (s, 1H), 6.16 (s, 2H), 5.29 (s, 2H), 4.90 (t, J = 6.5 Hz, 2H), 4.07 (s, 3H), 3.18 (t, J = 6.5 Hz, 2H), 2.88 (dt, J = 14.7, 7.4 Hz, 1H), 1.17 (d, J = 7.1 Hz, 6H). ^{13}C NMR (126 MHz, DMSO-d_6):

δ 150.9, 150.0, 148.9, 147.9, 145.5, 142.3, 137.5, 134.1, 133.1, 130.8, 129.2, 126.8, 126.4, 123.9, 122.0, 120.6, 120.4, 108.6, 105.6, 102.3, 75.5, 57.3, 55.5, 33.4, 26.5, 24.0. HRMS $[M+H]^+$: 454.2012 (calculated for: $[C_{29}H_{28}NO_4]^+$ 454.2013)

5.1.2.6 9-*O*-(3,5-dimethylbenzyl)berberine bromide (4f)

Yield 54%; mp 199-202 °C; ^{1}H NMR (500 MHz, DMSO-d_6): *δ* 9.71 (s, 1H), 8.94 (s, 1H), 8.20 (d, *J* = 9.0 Hz, 1H), 8.01 (d, *J* = 9.0 Hz, 1H), 7.77 (s, 1H), 7.18 (s, 2H), 7.07 (s, 1H), 6.97 (s, 1H), 6.16 (s, 2H), 5.24 (s, 2H), 4.92 (t, 2H), 4.08 (s, 3H), 3.18 (t, *J* = 6.2 Hz, 2H), 2.27 (s, 6H). ^{13}C NMR (126 MHz, DMSO-d_6): *δ* 151.0, 150.0, 147.9, 145.5, 142.3, 137.6, 137.5, 136.5, 133.1, 130.8, 129.9, 126.7, 124.0, 122.0, 120.6, 120.4, 108.6, 105.6, 102.3, 75.7, 57.2, 55.5, 26.6, 21.1. HRMS $[M+H]^+$: 440.1855 (calculated for: $[C_{28}H_{26}NO_4]$+ 440.1856)

5.1.2.7 9-O-(4-brombenzyl)berberine bromide (4g)

Yield 7%; mp 222-224 °C; ^{1}H NMR (500 MHz, DMSO-d_6): *δ* 9.79 (s, 1H), 8.94 (s, 1H), 8.18 (d, *J* = 9.1 Hz, 1H), 8.00 (d, *J* = 9.1 Hz, 1H), 7.76 (s, 1H), 7.61 – 7.55 (m, 4H), 7.07 (s, 1H), 6.15 (s, 2H), 5.32 (s, 2H), 4.94 (t, *J* = 6.2 Hz, 2H), 4.06 (s, 3H), 3.19 (t, *J* = 6.2 Hz, 2H). ^{13}C NMR (126 MHz, DMSO-d_6): *δ* 150.7, 150.0, 147.8, 145.5, 142.0, 137.6, 136.1, 133.1, 131.5, 131.1, 131.0, 130.8, 128.7, 126.6, 124.0, 121.8, 121.7, 120.6, 120.4, 108.6, 105.6, 102.3, 74.6, 57.2, 55.5, 26.5. HRMS $[M+H]^+$: 490.0650 (calculated for: $[C_{26}H_{21}BrNO_4]^+$ 490.0648)

5.1.2.8 9-*O*-(3-brombenzyl)berberine bromide (4h)

Yield 58%; mp 205-208 °C; ^{1}H NMR (500 MHz, DMSO-d_6): *δ* 9.83 (s, 1H), 8.94 (s, 1H), 8.19 (d, *J* = 9.1 Hz, 1H), 8.01 (d, *J* = 9.1 Hz, 1H), 7.85 (t, *J* = 1.8 Hz, 1H), 7.76 (s, 1H), 7.59 (d, *J* = 7.6 Hz, 1H), 7.55 (dd, *J* = 7.9, 2.0 Hz, 1H), 7.37 (t, *J* = 7.9 Hz, 1H), 7.07 (s, 1H), 6.16 (s, 2H), 5.32 (s, 2H), 4.94 (t, *J* = 6.3 Hz, 2H), 4.06 (s, 3H), 3.19 (t, *J* = 6.3 Hz, 2H). ^{13}C NMR (126 MHz, DMSO-d_6): *δ* 150.9, 150.0, 147.8, 145.5, 141.9, 139.4, 137.6, 133.1, 131.4, 131.3, 130.8, 130.8, 127.8, 126.6, 124.2, 121.9, 121.7, 120.6, 120.4, 108.6, 105.6, 102.3, 74.5, 57.2, 55.5, 26.5. HRMS $[M+H]^+$: 490.0649 (calculated for: $[C_{26}H_{21}BrNO_4]^+$ 490.0648)

5.1.2.9 9-*O*-(2-brombenzyl)berberine bromide (4i)

Yield 50%; mp 194-197 °C; ^{1}H NMR (500 MHz, DMSO-d_6): *δ* 9.83 (s, 1H), 8.94 (s, 1H), 8.20 (d, *J* = 9.2 Hz, 1H), 8.01 (d, *J* = 9.2 Hz, 1H), 7.85 (t, *J* = 1.8 Hz, 1H), 7.77 (s, 1H), 7.61 – 7.58 (m,

1H), 7.58 – 7.54 (m, 1H), 7.37 (t, *J* = 7.8 Hz, 1H), 7.07 (s, 1H), 6.16 (s, 2H), 5.32 (s, 2H), 4.94 (t, *J* = 6.3 Hz, 2H), 4.06 (s, 3H), 3.20 (t, *J* = 6.3 Hz, 2H). ^{13}C NMR (126 MHz, DMSO-d_6): δ 150.9, 150.0, 147.9, 145.5, 141.9, 139.4, 137.6, 133.1, 131.4, 131.3, 130.8, 130.8, 127.8, 126.6, 124.2, 121.9, 121.7, 120.6, 120.4, 108.6, 105.6, 102.3, 74.5, 57.2, 55.5, 26.5. HRMS $[M+H]^+$: 490.0637 (calculated for: $[C_{26}H_{21}BrNO_4]^+$ 490.0648)

5.1.2.10 9-*O*-(4-nitrobenzyl)berberine bromide (4j)

Yield 33%; mp 226-228 °C; ^{1}H NMR (500 MHz, DMSO-d_6): δ 9.84 (s, 1H), 8.94 (s, 1H), 8.19 (d, *J* = 9.1 Hz, 1H), 8.01 (d, *J* = 9.1 Hz, 1H), 7.87 – 7.84 (m, 1H), 7.76 (s, 1H), 7.62 – 7.53 (m, 2H), 7.37 (t, *J* = 7.8 Hz, 1H), 7.07 (s, 1H), 6.15 (s, 2H), 5.32 (s, 2H), 4.94 (t, *J* = 6.4 Hz, 2H), 4.06 (s, 3H), 3.19 (t, *J* = 6.4 Hz, 2H). ^{13}C NMR (126 MHz, DMSO-d_6): δ 150.8, 150.0, 147.8, 145.5, 141.9, 139.4, 137.6, 133.1, 131.4, 131.3, 130.8, 130.7, 127.8, 126.6, 124.2, 121.9, 121.7, 120.5, 120.4, 108.6, 105.6, 102.3, 74.5, 57.2, 55.5, 26.5. HRMS $[M+H]^+$: 457.1394 (calculated for: $[C_{26}H_{21}N_2O_6]^+$ 457.1394)

5.1.2.11 9-*O*-(4-methylthiobenzyl)berberine bromide (4k)

Yield 57%; mp 205-207 °C; ^{1}H NMR (500 MHz, DMSO-d_6): δ 9.73 (s, 1H), 8.94 (s, 1H), 8.20 (d, *J* = 9.2 Hz, 1H), 8.00 (d, *J* = 9.2 Hz, 1H), 7.78 (s, 1H), 7.55 – 7.51 (m, 2H), 7.28 – 7.24 (m, 2H), 7.08 (s, 1H), 6.17 (s, 2H), 5.32 (s, 2H), 4.92 (t, *J* = 6.4 Hz, 2H), 4.08 (s, 3H), 3.20 (t, *J* = 6.4 Hz, 2H), 2.46 (s, 3H). ^{13}C NMR (126 MHz, DMSO-d_6): δ 150.8, 150.0, 147.8, 145.5, 142.1, 138.8, 137.5, 133.1, 133.0, 130.8, 129.8, 126.7, 125.7, 123.9, 122.0, 120.5, 120.4, 108.6, 105.6, 102.3, 75.1, 57.2, 56.2, 55.5, 26.5, 14.7. HRMS $[M+H]^+$: 458.1418 (calculated for: $[C_{27}H_{24}NO_4S]^+$ 458.1421)

5.1.2.12 9-*O*-(3-nitrobenzyl)berberine bromide (4l)

Yield 65%; mp 201-204 °C; ^{1}H NMR (500 MHz, DMSO-d_6): δ 9.91 (s, 1H), 8.97 (s, 1H), 8.52 – 8.48 (m, 1H), 8.26 – 8.20 (m, 2H), 8.09 – 8.02 (m, 2H), 7.79 (s, 1H), 7.74 (t, *J* = 7.9 Hz, 1H), 7.09 (s, 1H), 6.17 (s, 2H), 5.48 (s, 2H), 4.95 (t, *J* = 6.4 Hz, 2H), 4.08 (s, 3H), 3.21 (t, *J* = 6.4 Hz, 2H). ^{13}C NMR (126 MHz, DMSO-d_6): δ 150.8, 150.0, 147.9, 147.8, 145.5, 141.9, 139.1, 137.7, 135.1, 133.1, 130.8, 130.2, 126.6, 124.3, 123.3, 123.1, 121.8, 120.6, 120.4, 108.6, 105.6, 102.3, 74.2, 57.2, 55.5, 26.5. HRMS $[M+H]^+$: 457.1392 (calculated for: $[C_{26}H_{21}N_2O_6]^+$ 457.1394)

5.1.2.13 9-*O*-(3-chlorbenzyl)berberine bromide (4m)

Yield 47%; mp 205-207 °C; ^{1}H NMR (500 MHz, CD_3OD): δ 9.63 (s, 1H), 8.70 (s, 1H), 8.15 (d, J = 9.1 Hz, 1H), 8.03 (d, J = 9.1 Hz, 1H), 7.66 (s, 1H), 7.65 – 7.62 (m, 1H), 7.48 – 7.43 (m, 1H), 7.39 – 7.32 (m, 2H), 6.96 (s, 1H), 6.11 (s, 2H), 5.44 (s, 2H), 4.89 (t, J = 6.4 Hz, 2H), 4.15 (s, 3H), 3.24 (t, J = 6.4 Hz, 2H). ^{13}C NMR (126 MHz, CD_3OD): δ 151.0, 150.8, 148.5, 144.8, 138.9, 134.0, 133.7, 130.5, 129.8, 128.4, 128.2, 126.7, 126.3, 123.7, 122.4, 120.4, 120.2, 110.0, 108.0, 105.1, 102.3, 74.6, 56.2, 55.9, 48.4, 26.8. HRMS $[M+H]^+$: 446.1152 (calculated for: $[C_{26}H_{21}ClNO_4]^+$ 446.1154)

5.1.2.14 9-*O*-(4-chlorbenzyl)berberine bromide (4n)

Yield 39%; mp 202-204 °C; ^{1}H NMR (500 MHz, DMSO-d_6): δ 9.79 (s, 1H), 8.95 (s, 1H), 8.20 (d, J = 9.2 Hz, 1H), 8.01 (d, J = 9.2 Hz, 1H), 7.78 (s, 1H), 7.66 – 7.63 (m, 2H), 7.49 – 7.45 (m, 2H), 7.09 (s, 1H), 6.17 (s, 2H), 5.35 (s, 2H), 4.94 (t, J = 6.4 Hz, 2H), 3.33 (s, 3H), 3.20 (t, J = 6.4 Hz, 2H). ^{13}C NMR (126 MHz, DMSO-d_6): δ 150.7, 150.0, 147.8, 145.5, 142.0, 137.6, 135.7, 133.1, 133.1, 130.8, 130.7, 128.5, 126.6, 124.0, 121.9, 120.5, 120.4, 108.6, 105.6, 102.3, 74.6, 57.2, 55.5, 48.7, 26.5. HRMS $[M+H]^+$: 446.1151 (calculated for: $[C_{26}H_{21}ClNO_4]^+$ 446.1154)

5.1.2.15 9-*O*-(3,4-dichlorbenzyl)berberine bromide (4o)

Yield 91%; mp 206-209 °C; ^{1}H NMR (300 MHz, DMSO-d_6): δ 9.85 (s, 1H), 8.94 (s, 1H), 8.20 (d, J = 9.2 Hz, 1H), 8.01 (d, J = 9.2 Hz, 1H), 7.91 (d, J = 2.0 Hz, 1H), 7.77 (s, 1H), 7.69 (s, 1H), 7.63 – 7.55 (m, 1H), 7.07 (s, 1H), 6.16 (s, 2H), 5.32 (s, 2H), 4.93 (t, J = 6.4 Hz, 2H), 4.05 (s, 3H), 3.20 (t, J = 6.4 Hz, 2H). ^{13}C NMR (75 MHz, DMSO-d_6): δ 150.8, 150.0, 147.9, 145.5, 141.8, 137.9, 137.7, 133.1, 131.2, 131.0, 130.9, 130.8, 130.6, 129.0, 126.6, 124.2, 121.8, 120.6, 120.4, 108.6, 105.6, 102.3, 73.9, 57.3, 55.5, 26.5. HRMS $[M+H]^+$: 480.0761 (calculated for: $[C_{26}H_{20}Cl_2NO_4]^+$ 480.0764

5.1.2.16 9-*O*-(4-methyloxykarbonyl)berberine bromide (4p)

Yield 59%; mp 203-205 °C; ^{1}H NMR (500 MHz, DMSO-d_6): δ 9.83 (s, 1H), 8.96 (s, 1H), 8.21 (d, J = 9.1 Hz, 1H), 8.02 (d, J = 8.7 Hz, 2H), 8.00 (d, J = 1.7 Hz, 1H), 7.79 (s, 1H), 7.76 (d, J = 8.0 Hz, 2H), 7.09 (s, 1H), 6.17 (s, 2H), 5.44 (s, 2H), 4.95 (t, J = 6.3 Hz, 2H), 4.07 (s, 3H), 3.86 (s, 3H), 3.20 (t, J = 6.3 Hz, 2H). ^{13}C NMR (126 MHz, DMSO-d_6): δ 166.1, 150.7, 150.0, 147.8, 145.5,

142.2, 142.0, 137.6, 133.1, 130.8, 129.5, 129.4, 128.6, 126.7, 124.1, 121.8, 120.6, 120.4, 108.6, 105.6, 102.3, 74.7, 57.2, 55.5, 52.4, 48.7, 26.5. HRMS $[M+H]^+$: 470.1599 (calculated for: $[C_{28}H_{24}NO_6]^+$ 470.1598)

5.1.2.17 9-*O*-(4-kyanbenzyl)berberine bromide (4q)

Yield 62%; mp 204-206 °C; ^{1}H NMR (500 MHz, DMSO-d_6): δ 9.84 (s, 1H), 8.96 (s, 1H), 8.22 (dd, *J* = 9.2, 1.5 Hz, 1H), 8.03 (d, *J* = 9.2 Hz, 1H), 7.91 (d, *J* = 8.2 Hz, 2H), 7.82 (d, J = 8.0 Hz, 2H), 7.80 (m, 1H), 7.09 (s, 1H), 6.17 (s, 2H), 5.44 (s, 2H), 4.94 (t, *J* = 6.3 Hz, 2H), 4.06 (s, 3H), 3.21 (t, *J* = 6.3 Hz, 2H). ^{13}C NMR (126 MHz, DMSO-d_6): δ 150.7, 150.0, 147.9, 145.5, 142.4, 141.9, 137.7, 133.1, 132.5, 130.9, 129.1, 126.7, 124.2, 121.7, 120.6, 120.4, 118.9, 111.1, 108.6, 105.6, 102.3, 74.4, 57.3, 55.5, 48.8, 26.5. HRMS $[M+H]^+$: 437.1495 (calculated for: $[C_{27}H_{21}N_2O_4]^+$ 437.1496)

5.1.2.18 9-*O*-(3-methoxybenzyl)berberine bromide (4r)

Yield 48%; mp 184-187 °C; ^{1}H NMR (500 MHz, DMSO-d_6): δ 9.79 (s, 1H), 8.94 (s, 1H), 8.20 (d, *J* = 9.1 Hz, 1H), 8.01 (d, *J* = 9.1 Hz, 1H), 7.78 (s, 1H), 7.32 – 7.27 (m, 1H), 7.21 – 7.18 (m, 1H), 7.15 – 7.11 (m, 1H), 7.08 (s, 1H), 6.92 – 6.89 (m, 1H), 6.17 (s, 2H), 5.33 (s, 2H), 4.93 (t, *J* = 6.4 Hz, 2H), 4.09 (s, 3H), 3.77 (s, 3H), 3.19 (t, *J* = 6.4 Hz, 2H). ^{13}C NMR (126 MHz, DMSO-d_6): δ 159.7, 151.1, 150.3, 148.1, 145.8, 142.4, 138.4, 137.8, 133.4, 131.1, 129.9, 127.0, 124.2, 122.3, 121.3, 120.9, 120.7, 114.6, 114.5, 108.9, 105.9, 102.6, 75.7, 57.5, 55.8, 55.6, 26.8. HRMS $[M+H]^+$: 442.1645 (calculated for: $[C_{27}H_{24}NO_5]^+$ 442.1649)

5.1.2.19 9-*O*-(4-trifluormethylbenzyl)berberine bromide (4s)

Yield 62%; mp 206-209 °C; ^{1}H NMR (500 MHz, DMSO-d_6): δ 9.85 (s, 1H), 8.97 (s, 1H), 8.21 (d, *J* = 9.2 Hz, 1H), 8.03 (d, *J* = 9.2 Hz, 1H), 7.86 (d, *J* = 8.1 Hz, 2H), 7.81 (s, 1H), 7.79 (s, 2H), 7.09 (s, 1H), 6.17 (s, 2H), 5.45 (s, 2H), 4.95 (t, *J* = 6.4 Hz, 2H), 4.07 (s, 3H), 3.21 (t, *J* = 6.4 Hz, 2H). ^{13}C NMR (126 MHz, DMSO-d_6): δ 151.0, 150.3, 148.1, 145.8, 142.3, 141.9, 137.9, 133.4, 131.1, 129.4, 127.0, 125.7, 125.7, 125.7, 125.7, 124.4, 122.0, 120.8, 120.7, 108.9, 105.9, 102.6, 74.8, 57.5, 55.8, 26.8. HRMS $[M+H]^+$: 480.1415 (calculated for: $[C_{27}H_{21}F_3NO_4]^+$ 480.1417)

5.1.2.20 9-*O*-(4-methoxybenzyl)berberine bromide (4t)

Yield 88%; mp 196-198 °C; ^{1}H NMR (500 MHz, DMSO-d_6): δ 9.70 (s, 1H), 8.93 (s, 1H), 8.19 (d, J = 9.2 Hz, 1H), 7.99 (d, J = 9.2 Hz, 1H), 7.77 (s, 1H), 7.54 – 7.49 (m, 2H), 7.08 (s, 1H), 6.95 – 6.90 (m, 2H), 6.17 (s, 2H), 5.29 (s, 2H), 4.92 (t, J = 6.4 Hz, 2H), 4.09 (s, 3H), 3.74 (s, 3H), 3.19 (t, J = 6.4 Hz, 2H). ^{13}C NMR (126 MHz, DMSO-d_6): δ 159.6, 150.9, 150.0, 147.8, 145.5, 142.1, 137.4, 133.0, 130.9, 130.8, 128.5, 126.6, 123.8, 122.1, 120.5, 120.4, 113.8, 108.6, 105.6, 102.2, 75.2, 57.2, 55.5, 55.3, 26.5. HRMS $[M+H]^+$: 442.1646 (calculated for: $[C_{27}H_{24}NO_5]^+$ 442.1649)

5.1.2.21 9-*O*-(napht-2-yl)berberine bromide (4u)

Yield 55%; mp 212-214 °C; ^{1}H NMR (500 MHz, DMSO-d_6): δ 9.82 (s, 1H), 8.93 (s, 1H), 8.22 (d, J = 9.2 Hz, 1H), 8.11 – 8.08 (m, 1H), 8.01 (d, J = 9.2 Hz, 1H), 7.98 – 7.91 (m, 3H), 7.80 – 7.76 (m, 2H), 7.56 – 7.51 (m, 2H), 7.08 (s, 1H), 6.17 (s, 2H), 5.53 (s, 2H), 4.92 (t, J = 6.4 Hz, 2H), 4.11 (s, 3H), 3.16 (t, J = 6.4 Hz, 2H). ^{13}C NMR (126 MHz, DMSO-d_6): δ 150.9, 150.0, 147.8, 145.5, 142.2, 137.5, 134.2, 133.1, 132.9, 132.8, 130.8, 128.1, 128.1, 127.8, 127.7, 126.7, 126.7, 126.5, 126.5, 123.9, 122.0, 120.5, 120.4, 108.6, 105.6, 102.3, 75.6, 57.3, 55.5, 26.5. HRMS $[M+H]^+$: 462.1697 (calculated for: $[C_{30}H_{24}NO_4]^+$ 462.1700)

5.1.2.22 *rac*-9-*O*-(α-methylbenzyl)berberine bromide (4v)

Yield 20%; mp 195-198 °C; ^{1}H NMR (500 MHz, DMSO-d_6): δ 9.74 (s, 1H), 8.90 (s, 1H), 8.13 (d, J = 9.1 Hz, 1H), 7.92 (d, J = 9.1 Hz, 1H), 7.77 (s, 1H), 7.57 – 7.53 (m, 2H), 7.34 – 7.27 (m, 3H), 7.27 – 7.22 (m, 1H), 7.08 (s, 1H), 6.17 (s, 2H), 5.92 – 5.86 (m, 1H), 5.03 – 4.90 (m, 2H), 4.04 (s, 3H), 3.25 – 3.14 (m, 2H), 1.73 (d, J = 6.5 Hz, 3H). ^{13}C NMR (126 MHz, DMSO-d_6): δ 150.5, 150.0, 147.8, 145.4, 141.3, 141.1, 137.5, 133.0, 130.8, 128.4, 128.4, 127.2, 126.6, 123.4, 122.4, 120.6, 120.4, 108.6, 105.6, 102.3, 80.7, 57.1, 55.4, 26.5. HRMS $[M+H]^+$: 426.1697 (calculated for: $[C_{27}H_{24}NO_4]^+$ 426.1700)

5.2 Inhibition of human AChE and BChE

The AChE and BChE inhibitory activities of the tested compounds were determined using a modified Ellman´s method [52]. Human recombinant acetylcholinesterase (*h*AChE; EC 3.1.1.7), human plasmatic butyrylcholinesterase (*h*BChE; EC 3.1.1.8), 5,5´-dithiobis(2-nitrobenzoic acid) (Ellman´s reagent, DTNB), phosphate buffer (PB; 0.1M KH_2PO_4/K_2HPO_4 buffer, pH 7.4), acetylthiocholine iodide (ATCh), and butyrylthiocholine

iodide (BTCh) were purchased from Sigma-Aldrich (Prague, Czech Republic). For measuring purposes – polystyrene Nunc 96-well microplates with flat bottom shape (ThermoFisher Scientific, USA) were utilized. All of the assays were carried out in. Enzyme solutions were prepared at an activity 2.0 units·mL^{-1} in 2 mL aliquots. The assay medium (100 µL) consisted of 40 µL of 0.1 M PB, 20 µL of 0.01 M DTNB, 10 µL of the enzyme, and 20 µL of 0.01 M substrate (ATCh or BTCh iodide solution). Assayed solutions with inhibitors (10 µL, 10^{-3}-10^{-9} M) were preincubated with *h*AChE or *h*BChE for 5 min. The reaction was started by the addition of 20 µL of the substrate. The enzyme activity was determined by measuring the increase in absorbance at 412 nm at 37°C in 2 min intervals using a Multimode microplate reader Synergy 2 (Vermont, USA). Each concentration was assayed in triplicate. The obtained data were used to compute the percentage of inhibition (*I*; Eq. 2):

$$I = \left(1 - \frac{\Delta A_i}{\Delta A_0}\right) \times 100 \quad [\%] \quad \text{(Equation 2)}$$

ΔA_i indicates absorbance change provided by the cholinesterase exposed to AChE inhibitors. ΔA_0 indicates absorbance change caused by the intact cholinesterase (phosphate buffer was used instead of the AChE inhibitor solution). Inhibition potency of tested compounds was expressed as the IC_{50} value (the concentration of inhibitor, which causes 50% cholinesterase inhibition). All calculations were performed using Microsoft Excel software (Redmont, WA, USA) and GraphPad Prism version 5.02 for Windows (GraphPad Software, San Diego, CA) (www.graphpad.com).

5.3 Prolyl oligopeptidase inhibition

Recombinant POP was purchased from Sigma-Aldrich (Prague, Czech Republic). POP was dissolved in phosphate buffered saline (PBS; 0.01 M Na/K phosphate buffer, pH 7.4, containing 137 mM NaCl and 2.7 mM KCl); the specific activity of the enzyme was 0.2 U/mL. The assays were performed in standard polystyrene 96-well microplates with a flat and clear bottom. Stock solutions of tested compounds were prepared in DMSO (10 mM). Dilutions (10^{-3}M - 10^{-7} M) were prepared from the stock solution with deionized H_2O; the control was performed with the same DMSO concentration. POP substrate, (*Z*)-Gly-Pro-*p*-nitroanilide, was dissolved in 50% 1,4-dioxane (5 mM). For each reaction, PBS (170 µL), tested compound (5µL), and POP (5µL) were incubated for 5 min at 37°C. Then, the substrate (20 µL) was added and the microplate was incubated for 30 min at 37°C. The formation of *p*-nitroanilide,

directly proportional to the POP activity, was measured spectrophotometrically at 405 nm using a Multimode microplate reader Synergy 2 (Vermont, USA). Inhibition potency of the tested compounds was expressed as IC_{50} value (concentration of inhibitor, which causes 50% POP inhibition).

5.4 Kinetic study of AChE and BChE inhibition

The kinetic study of AChE and BChE was performed by using the above-mentioned modified Ellman's method [52]. The values of V_{max} and K_m of the Michaelis-Menten kinetics as well as the values of K_i and K_i' were calculated by nonlinear regression from the substrate velocity curves. Linear regression was used for the calculation of Lineweaver-Burk plots. All calculations were performed using GraphPad Prism software version 6.07 forWindows (San Diego, CA, USA).

5.5 Molecular modeling studies

From the online PDB database (www.rcsb.org) models of *h*AChE (PDB ID: 4EY6, resolution: 2.40 Å), *h*BChE (PDB ID: 4BDS, resolution: 2.10 Å) and POP (PDB ID: 3DDU, resolution: 1.56 Å) were downloaded and prepared for flexible molecular docking by Chimera DockPrep (v. 1.4)[88] and MGL Tools utilities [89–91]. The preparation of these receptors involved removal of the surplus copies of the enzyme chains, non-bonded inhibitors, addition of polar hydrogens and merging of non-polar ones. Default Gasteiger charges were assigned to all atoms. Flexible parts of the enzymes were determined based on previous experiences. Around the selected flexible residues, grid boxes of 40 × 50 × 40 Å for *h*AChE and *h*BChE and 60 × 50 × 45 Å for POP were positioned. The rotatable bonds in the flexible residues were detected automatically by AutoDock Tools 1.5.4 program. Given the limitation of the program used for flexible molecular docking, water molecules had to be removed from the system. The flexible receptor parts contained 40 residues for *h*AChE, 39 residues for *h*BChE and 15 residues for POP. Following xyz coordinates of the grid box centers were applied: *h*AChE (10.698, -58.115, -23.192); *h*BChE (140.117, 122.247, 38.986); POP (-4.5, 11.7, 31.6). The studied ligands were firstly drawn in HyperChem 8.0, then manually protonated as suggested by MarvinSketch 6.2.0. software (http://www.chemaxon.com), geometrically optimized by software Avogadro (v. 1.2.0) using the Generalized Amber Force Field. [92] Molecular docking was carried out in AutoDock Vina 1.1.2 program utilizing computer resources of the Czech National Grid Infrastructure MetaCentrum. The search algorithm of AutoDock Vina efficiently combines a Markov chain Monte Carlo like the method for the

global search and a Broyden-Fletcher-Goldfarb-Shano gradient approach for the local search [93]. It is a type of memetic algorithm based on interleaving stochastic and deterministic calculations [94]. Each docking task was repeated 15 times with the exhaustiveness parameter set to 16, employing 16 CPU in parallel multithreading. The procedure was tested by re-docking of co-crystallized ligands, and it was found as suitable. From the obtained results, the solutions reaching the minimum predicted Gibbs binding energy was taken as the top-scoring modes. The graphic representations of the docked poses were rendered in PyMOL (The PyMOL Molecular Graphics System, Version 1.5.0.4 Schrödinger, LLC.). 2D diagrams were generated using Discovery Studio Visualizer v16.1.0.15350 (Dassault Systèmes Biovia Corp., 2016, San Diego, USA).

5.6 QSAR analyses

Molecular models of the studied ligands **4a**-**4v** were prepared in Schrodinger 2020-1 and geometrically optimized by semiempirical quantum chemistry method PM3, applying the default optimization algorithm. All ligands were modeled as charged molecules with multiplicity set to 1. Besides geometrical optimization, calculation of electrostatic charges, electron affinity, ionization energy and SAR properties was performed for each ligand. Such ligand set was investigated by DeepChem and AutoQSAR tools to discover statistically significant QSAR models. In AutoQSAR, calculation of radial, linear, dendritic and molprint 2D fingerprints was performed. In addition, Canvas molecular descriptors were calculated and investigated by multiple linear regression, principal component analysis and kernel partial least square regression with automatic optimization and selection of the best model. The independent variables were used in their decadic logarithm form. All statistical analyses were performed in the AutoQSAR tool. For the calculations, a high-performance computer cluster with 1776 CPUs was employed.

5.7 Evaluation of cytotoxicity by MTT assay

The standard 3-(4,5-dimethylthiazol-2-yl)-2,5-diphenyltetrazolium bromide (MTT) cell viability assay (Merck, Prague, Czech Republic) was applied according to the manufacturer's protocol on the Chinese hamster ovary cell line CHO-K1 (ECACC, Salisbury, UK) in order to compare the effect of different compound within the series [68]. The cells were cultured according to ECACC recommended conditions and seeded in a density of 8×10^3 per well.

Tested compounds were dissolved in DMSO (Merck, Prague, Czech Republic) and subsequently in the growth medium (F-12) so that the final concentration of DMSO did not exceed 0.5% (v/v) per well. Cells were exposed to the tested compounds for 24 h. The medium was replaced by a medium containing 10 µM of MTT and cells were allowed to produce formazan for approximately 3 h under surveillance. Thereafter, the medium with MTT was sucked out and crystals of formazan were dissolved in DMSO (100 µL). Cell viability was assessed spectrophotometrically by the amount of formazan produced. Absorbance was measured at 570 nm with 650 nm as a reference wavelength on Synergy HT (BioTek, Vermont, USA). IC_{50} value was then calculated from the control – subtracted triplicates using non-linear regression (four parameters) of GraphPad Prism 5 software (GraphPad Software, Inc., San Diego, CA). Final IC_{50} and SEM value were obtained as a mean of three independent measurements.

5.8 Evaluation of antioxidant activity

Diphenyl-1-picrylhydrazyl stable free radical assay (DPPH) [95] is a simple method to determine antioxidant activity and is expressed as EC_{50}, that is, the concentration of compound that causes a 50% decrease in the DPPH activity. DPPH, methanol, and Trolox (as reference standard) were purchased from Sigma-Aldrich (Czech Republic). Polystyrene Nunc 96-well microplates with flat bottom shape (ThermoFisher Scientific, U.S.) were used for measuring purposes. All of the assays were carried out in methanol. DPPH solution was prepared at 0.2 mM concentration. The assay medium (200 µL) consisted of 100 µL of DPPH solution and 100 µL of tested compound (10^{-3}-10^{-6} M). The reaction time constituted 30 min. The antioxidant activity was determined by measuring the increase in absorbance at 517 nm at laboratory temperature using Multimode microplate reader Synergy 2 (Vermont) [96]. Each concentration was tested in triplicate. Software GraphPad Prism version 5 for Windows (GraphPad Software, San Diego, CA) was used for statistical data evaluation.

5.9 Determination of $A\beta_{1-42}$ self-aggregation inhibition

1 mg of $A\beta_{1-42}$ (HFIP-treated, Bachem, Weil am Rhein, Germany) was dissolved in DMSO to obtain a stable stock solution, aliquoted and stored at -20 °C. For the assay, $A\beta_{1-42}$ stock solution was then diluted to a final 50 µM concentration with 10 mM phosphate buffer (pH = 7.4) containing 150 mM NaCl by brief sonication and vortexing. 1 mg of thioflavin T (ThT) was dissolved in methanol to obtain a stock solution which was subsequently diluted in

50 mM glycine-NaOH (pH = 8.6) to 0.4 mM. Assay mixture contains 20 µM ThT. Stock solutions of inhibitors were prepared in DMSO.

$A\beta_{1-42}$ self-aggregation was performed by incubating of 50 µM $A\beta_{1-42}$ solution at 30 °C in the assay conditions without any stirring in a black, clear-bottom 96-well plate (Greiner) by a multi-plate reader (Synergy HT, Biotek, Winooski, Vermont, United States) using ThT fluorimetric assay. The final volume of assay mixture was 100 µL. The excitation and emission wavelengths were set at 440/30 and 485/20 nm, respectively. Inhibition experiments were monitored by incubating $A\beta_{1-42}$ at the given conditions in the presence of 50 µM studied berberine samples. As a positive control, 50 µM doxycycline was used. Fluorescence data were recorded every 10 min during 72 h incubation time without any stirring. Each inhibitor was assayed in duplicates in at least three independent experiments and the presented values were averaged and are expressed as the mean ± SEM (the standard error of the mean). First the ratio was calculated after subtraction of fluorescence of unbound ThT according to Eq. 3:

$$R=\frac{F_{plateau}-F_{lag}}{F_{lag}} \quad \text{(Equation 3)},$$

where F_{lag} and $F_{plateau}$ are fluorescence intensities of $A\beta_{1-42}$in lag and plateau phase of aggregation kinetic at five time points every 30 min, respectively. After that, the percent inhibition of$A\beta_{1-42}$ aggregation was calculated as follow (Eq. 4):

$$\%\ inhibition = 100 - \left(\frac{R_I}{R_0}\right) \times 100 \text{ (Equation 4)}$$

where R_I and R_0 are ratios according to Eq. 3 with or without studied compounds, respectively.

5.10 Determination of τ self-aggregation inhibition

$Tau_{306-336}$ samples were prepared by taking 1 mg of $\tau_{306-336}$ purchased from Bachem (Germany) and initially, it was dissolved in 1,1,1,3,3,3-hexafluoro-2-propanol (HFIP), gently vortexed, sonicated and kept overnight at room temperature (RT). Subsequently, the sample was aliquoted, evaporated, dried, and stored in -20 °C.

For the measurement of τ self-aggregation and its inhibition, $Tau_{306-336}$ peptide stock solution (500 µM) was freshly prepared by dissolving aliquot in ultrapure water. 500 µM thioflavin T (ThT) was prepared in 56.3 mM phosphate buffer (PB, pH = 7.4). $Tau_{306-336}$self-aggregation was measured using ThT fluorimetric assay with some variations [97]. For the measurement

were used following conditions – 20 µM ThT, 90/10 MeOH/DMSO (v/v), 56.3 mM PB and 25 µM $Tau_{306-336}$ in final 100 µL volume. Inhibition experiments were performed by incubating$Tau_{306-336}$peptide at given conditions in the presence of potential tested inhibitors at 25 µM. Fluorescence intensity was measured in black, clear bottom 96-well plate (Greiner) by Spark multi-plate reader (Tecan GmbH, Grödig, Austria). The excitation and emission wavelengths were set at 446 and 490 nm, respectively. Assays were performed at 30 °C. Fluorescence data were recorded every 10 min overnight with 1 min shaking at 800 rpm prior to each reading. All ThT fluorimetric experiments were performed in duplicates in at least three independent experiments. Estimation of the inhibitory potency (%) was carried out by comparing fluorescence values at the plateau (average fluorescence intensity value in the 14–18 h range). Values were averaged and the presented inhibition % values are expressed as the mean ± SEM.

5.11 Determination of *in vitro* BBB permeation

PAMPA (the parallel artificial membrane permeability assay) is a high-throughput screening tool applicable for prediction of the passive transport of potential drugs across the BBB) [98]. In this study, it has been used as a non-cell-based *in vitro* assay carried out in a coated 96-well membrane filter. The filter membrane of the donor plate was coated with PBL (Polar Brain Lipid, Avanti, USA) in dodecane (4 µl of 20 mg/mL PBL in dodecane) and the acceptor well was filled with 300 µL of phosphate buffer saline, (PBS pH 7.4; V_A). The tested compounds were dissolved first in DMSO and then diluted with PBS pH 7.4 to reach the final concentrations 50 - 500 µM in the donor well. The final concentration of DMSO did not exceed 0.5% (v/v) in the donor solution. 300 µL of the donor solution (V_D) was added to the donor wells and the donor filter plate was carefully put on the acceptor plate so that the coated membrane was “in touch” with both donor solution and acceptor buffer. In principle, test compound diffuse from the donor well through the polar brain lipid membrane (*Area* = 0.28 cm^2) to the acceptor well. The concentration of the tested compound in both donor and the acceptor wells were assessed after 3, 4, 5 and 6 hours of incubation respectively in quadruplicate using the UV plate reader Synergy HT (Biotek, USA) at the maximum absorption wavelength of each compound (n = 3). Besides that, the solution of theoretical compound concentration, simulating the equilibrium state established if the membrane were ideally permeable was prepared and assessed as well. The concentration of the compounds in the donor and acceptor well and equilibrium concentration were

calculated from the standard curve and expressed as the permeability (*Pe*) according to the Eq. 5 [98].

$$\log Pe = \log\left\{C \times -\ln\left(1 - \frac{[drug]_{acceptor}}{[drug]_{equilibrium}}\right)\right\}$$

$$\text{where } C = \left(\frac{V_D \times V_A}{(V_D + V_A) \times Area \times Time}\right). \qquad \text{(Equation 5)}$$

5.12 Statistical analysis

Calculation were performed using GraphPad Prism 6.05 (GraphPad Software, San Diego, USA) and Microsoft Excel 2010 (Microsoft Corporation, Redmond, USA) with PKsolver extension [99].

Appendix A. Supplementary data

Supplementary data related to this article can be found at…

Notes

The authors declare no competing financial interest.

Author Contributions

[#] Katerina Sobolova and Martina Hrabinova contributed equally.

Acknowledgment

The study was supported by a grant of Ministry of Defence "Long Term Development Plan" Medical Aspects of Weapons of Mass Destruction of the Faculty of Military Health Sciences, University of Defence; by the Ministry of Education, Youth and Sports of Czech Republic (project ERDF IT4N no. CZ.02.1.01/0.0/0.0/18_069/0010054), by EU COST Action (CA15135: "Multi-target paradigm for innovative ligand identification in the drug discovery process (MuTaLig)"), by Czech Science Foundation (no. 20-29633J), and by MH CZ - DRO (University Hospital Hradec Kralove, No. 00179906). Computational resources were provided by the CESNET LM2015042 and the CERIT Scientific Cloud LM2015085, provided under the programme "Projects of Large Research, Development, and Innovations Infrastructures". The QSAR studies were performed on a supercomputer Sofia of the University of Hradec Kralove.

Abbreviations

Aβ, amyloid-beta peptide; ACh, acetylcholine; AChE, acetylcholinesterase; AD, Alzheimer's disease; ΔA_0, absorbance change caused by the intact cholinesterase; ΔA_i, absorbance change provided by the cholinesterase exposed to AChE inhibitors; ATCh, acetylthiocholine; BBB, blood-brain barrier; BBR, berberine; BChE, butyrylcholinesterase; BTCh,

butyrylthiocholine; CAS, catalytic anionic site; CH_3Cl, chloroform; ChE, cholinesterase; CHO-K1, chinese hamster ovary; clogP, partition coefficient; DC-CNN QSAR, deep chemistry convolutional neural network quantitative structure-activity relationship; DMSO, dimethylsulfoxide; DPPH, 1,1-diphenyl-2-picryl-hydrazyl; DTNB, 5,5'-dithiobis(2-nitrobenzoic acid); EC, effective concentration; *h*AChE, human acetylcholinesterase; *h*BChE, human butyrylcholinesterase; HepG2, human liver carcinoma cell line; HFIP, 1,1,1,3,3,3-hexafluoro-2-propanol; HRMS, high-resolution mass spectra; IC, inhibitory concentration; Ins(1, 4, 5)P_3, inositol 1, 4, 5-triphosphate; K_2CO_3, potassium carbonate; KCl, potassium chloride; K_i, inhibition constant between inhibitor and enzyme-inhibitor complex; $K_{i'}$, inhibition constant between inhibitor and enzyme-inhibitor-substrate complex; K_m, Michaelis-Menten constant; kPLS, kernel partial least regression; LC-MS, liquid-chromatography-mass spectrometry; MeCN, acetonitrile; MeOH, methanol; mp, melting point; MTT, 3-(4,5-dimethylthiazol-2-yl)-2,5-diphenyl tetrazolium bromide; NaCl, sodium chloride; n.d., not determined; NMR, nuclear magnetic resonance; OS, oxidative stress; PAMPA, parallel artificial membrane permeation assay; PAS, peripheral anionic site; PB, phosphate buffer; PBL, polar brain lipid; PBS, phosphate buffer solution; P_e, permeability; POP, prolyl oligopeptidase; POPi, prolyl oligopeptidase inhibitor; QSAR, quantitative structure-activity relationship; SAR, structure-activity relationship; SEM, standard error of the mean; SI, selectivity index; τ, tau protein; THF, tetrahydrofuran; ThT, thioflavin; TLC, thin layer chromatography; V_A, colume of acceptor solution; V_D, volume of donor solution; V_{max}, maximum reaction velocity; v/v, percentage by volume.

References

[1] A. Smith, K. Kobayashi, N. Chappell, D. Hoxsey, The controversial promises of cholinesterase inhibitors for Alzheimer's disease and related dementias: A qualitative study of caregivers' experiences, J. Aging Stud. 25 (2011) 397–406. https://doi.org/10.1016/j.jaging.2011.03.002.

[2] A.D. International, World Alzheimer Report 2019: Attitudes to dementia | Alzheimer's Disease International, (2019). https://www.alz.co.uk/research/world-report-2019 (accessed June 15, 2020).

[3] Alzheimer's Association, Alzheimer's Disease & Dementia | Alzheimer's Association, Alzheimers Assoc. (2015). http://www.alz.org/alzheimers_disease_what_is_alzheimers.asp (accessed February 18, 2015).

[4] S. Kumar, E.J. Okello, J.R. Harris, Experimental Inhibition of Fibrillogenesis and Neurotoxicity by amyloid-beta (Aβ) and Other Disease-Related Peptides/Proteins by

Plant Extracts and Herbal Compounds, in: J.R. Harris (Ed.), Protein Aggreg. Fibrillogenesis Cereb. Syst. Amyloid Dis., Springer Netherlands, 2012: pp. 295–326. http://link.springer.com/chapter/10.1007/978-94-007-5416-4_13 (accessed March 9, 2015).

[5] H. Dubey, K. Gulati, A. Ray, Recent studies on cellular and molecular mechanisms in Alzheimer's disease: focus on epigenetic factors and histone deacetylase, Rev. Neurosci. 29 (2018) 241–260. https://doi.org/10.1515/revneuro-2017-0049.

[6] M. Medina, J. Avila, New perspectives on the role of tau in Alzheimer's disease. Implications for therapy, Biochem. Pharmacol. 88 (2014) 540–547. https://doi.org/10.1016/j.bcp.2014.01.013.

[7] H.-F. Ji, L. Shen, Berberine: a potential multipotent natural product to combat Alzheimer's disease, Mol. Basel Switz. 16 (2011) 6732–6740. https://doi.org/10.3390/molecules16086732.

[8] M.T. Lin, M.F. Beal, Mitochondrial dysfunction and oxidative stress in neurodegenerative diseases, Nature. 443 (2006) 787–795. https://doi.org/10.1038/nature05292.

[9] A. Nunomura, R.J. Castellani, X. Zhu, P.I. Moreira, G. Perry, M.A. Smith, Involvement of oxidative stress in Alzheimer disease, J. Neuropathol. Exp. Neurol. 65 (2006) 631–641. https://doi.org/10.1097/01.jnen.0000228136.58062.bf.

[10] S. Menazza, B. Blaauw, T. Tiepolo, L. Toniolo, P. Braghetta, B. Spolaore, C. Reggiani, F. Di Lisa, P. Bonaldo, M. Canton, Oxidative stress by monoamine oxidases is causally involved in myofiber damage in muscular dystrophy, Hum. Mol. Genet. 19 (2010) 4207–4215. https://doi.org/10.1093/hmg/ddq339.

[11] M.B.H. Youdim, D. Edmondson, K.F. Tipton, The therapeutic potential of monoamine oxidase inhibitors, Nat. Rev. Neurosci. 7 (2006) 295–309. https://doi.org/10.1038/nrn1883.

[12] E. Giacobini, Cholinergic foundations of Alzheimer's disease therapy, J. Physiol.-Paris. 92 (1998) 283–287. https://doi.org/10.1016/S0928-4257(98)80034-X.

[13] N.C. Inestrosa, A. Alvarez, C.A. Pérez, R.D. Moreno, M. Vicente, C. Linker, O.I. Casanueva, C. Soto, J. Garrido, Acetylcholinesterase accelerates assembly of amyloid-beta-peptides into Alzheimer's fibrils: possible role of the peripheral site of the enzyme, Neuron. 16 (1996) 881–891.

[14] A. Nordberg, C. Ballard, R. Bullock, T. Darreh-Shori, M. Somogyi, A Review of Butyrylcholinesterase as a Therapeutic Target in the Treatment of Alzheimer's Disease, Prim. Care Companion CNS Disord. 15 (2013) 0–0. https://doi.org/10.4088/PCC.12r01412.

[15] J.B. Standridge, Pharmacotherapeutic approaches to the treatment of Alzheimer's disease, Clin. Ther. 26 (2004) 615–630. https://doi.org/10.1016/S0149-2918(04)90064-1.

[16] M. Kamori, M. Hagihara, T. Nagatsu, H. Iwata, T. Miura, Activities of dipeptidyl peptidase II, dipeptidyl peptidase IV, prolyl endopeptidase, and collagenase-like peptidase in synovial membrane from patients with rheumatoid arthritis and osteoarthritis, Biochem. Med. Metab. Biol. 45 (1991) 154–160.

[17] A. Penttinen, J. Tenorio-Laranga, A. Siikanen, M. Morawski, S. Rossner, J.A. García-Horsman, Prolyl oligopeptidase: a rising star on the stage of neuroinflammation research, CNS Neurol. Disord. Drug Targets. 10 (2011) 340–348.

[18] A. Gaggar, P.L. Jackson, B.D. Noerager, P.J. O'Reilly, D.B. McQuaid, S.M. Rowe, J.P. Clancy, J.E. Blalock, A Novel Proteolytic Cascade Generates an Extracellular Matrix-Derived Chemoattractant in Chronic Neutrophilic Inflammation, J. Immunol. Baltim. Md 1950. 180 (2008) 5662–5669.

[19] R. Kumar, S. Parameswaran, R. Bavi, A. Baek, M. Son, S. Rampogu, C. Park, G. Lee, A. Zeb, S. Parate, R.M. Rana, K.W. Lee, Investigation of novel chemical scaffolds targeting prolyl oligopeptidase for neurological therapeutics, J. Mol. Graph. Model. 88 (2019) 92–103. https://doi.org/10.1016/j.jmgm.2018.12.006.

[20] T. Aoyagi, T. Wada, M. Nagai, F. Kojima, S. Harada, T. Takeuchi, H. Takahashi, K. Hirokawa, T. Tsumita, Deficiency of kallikrein-like enzyme activities in cerebral tissue of patients with Alzheimer's disease, Experientia. 46 (1990) 94–97.

[21] N. Momeni, B.M. Nordström, V. Horstmann, H. Avarseji, B.V. Sivberg, Alterations of prolyl endopeptidase activity in the plasma of children with autistic spectrum disorders, BMC Psychiatry. 5 (2005) 27. https://doi.org/10.1186/1471-244X-5-27.

[22] J. Tenorio-Laranga, C. Montoliu, A. Urios, V. Hernandez-Rabaza, H. Ahabrach, J.A. García-Horsman, V. Felipo, The expression levels of prolyl oligopeptidase responds not only to neuroinflammation but also to systemic inflammation upon liver failure in rat models and cirrhotic patients, J. Neuroinflammation. 12 (2015) 183. https://doi.org/10.1186/s12974-015-0404-7.

[23] M. Maes, F. Goossens, S. Scharpé, J. Calabrese, R. Desnyder, H.Y. Meltzer, Alterations in plasma prolyl endopeptidase activity in depression, mania, and schizophrenia: effects of antidepressants, mood stabilizers, and antipsychotic drugs, Psychiatry Res. 58 (1995) 217–225.

[24] G. Larrinaga, I. Perez, L. Blanco, J.I. López, L. Andrés, C. Etxezarraga, F. Santaolalla, A. Zabala, A. Varona, J. Irazusta, Increased prolyl endopeptidase activity in human neoplasia, Regul. Pept. 163 (2010) 102–106. https://doi.org/10.1016/j.regpep.2010.03.012.

[25] I. Schulz, B. Gerhartz, A. Neubauer, A. Holloschi, U. Heiser, M. Hafner, H.-U. Demuth, Modulation of inositol 1,4,5-triphosphate concentration by prolyl endopeptidase inhibition, Eur. J. Biochem. 269 (2002) 5813–5820. https://doi.org/10.1046/j.1432-1033.2002.03297.x.

[26] K. Babkova, J. Korabecny, O. Soukup, E. Nepovimova, D. Jun, K. Kuca, Prolyl oligopeptidase and its role in the organism: attention to the most promising and clinically relevant inhibitors, Future Med. Chem. 9 (2017) 1015–1038. https://doi.org/10.4155/fmc-2017-0030.

[27] E. Proschak, H. Stark, D. Merk, Polypharmacology by Design: A Medicinal Chemist's Perspective on Multitargeting Compounds, J. Med. Chem. 62 (2019) 420–444. https://doi.org/10.1021/acs.jmedchem.8b00760.

[28] A. Cavalli, M.L. Bolognesi, A. Minarini, M. Rosini, V. Tumiatti, M. Recanatini, C. Melchiorre, Multi-target-directed ligands to combat neurodegenerative diseases, J. Med. Chem. 51 (2008) 347–372. https://doi.org/10.1021/jm7009364.

[29] O. Benek, J. Korabecny, O. Soukup, A Perspective on Multi-target Drugs for Alzheimer's Disease, Trends Pharmacol. Sci. 41 (2020) 434–445. https://doi.org/10.1016/j.tips.2020.04.008.

[30] D. Xiao, Z. Liu, S. Zhang, M. Zhou, F. He, M. Zou, J. Peng, X. Xie, Y. Liu, D. Peng, Berberine Derivatives with Different Pharmacological Activities via Structural

Modifications, Mini Rev. Med. Chem. 18 (2018) 1424–1441. https://doi.org/10.2174/1389557517666170321103139.

[31] I.V. Nechepurenko, U.A. Boyarskikh, N.I. Komarova, M.P. Polovinka, M.L. Filipenko, G.I. Lifshits, N.F. Salakhutdinov, G.A. Tolstikov, LDLR up-regulatory activity of berberine and its bromo and iodo derivatives in human liver HepG2 cells, Dokl. Chem. 439 (2011) 204–208. https://doi.org/10.1134/S0012500811070093.

[32] I.P. Singh, S. Mahajan, Berberine and its derivatives: a patent review (2009 – 2012), Expert Opin. Ther. Pat. 23 (2012) 215–231. https://doi.org/10.1517/13543776.2013.746314.

[33] T. Ahmed, A.-H. Gilani, M. Abdollahi, M. Daglia, S.F. Nabavi, S.M. Nabavi, Berberine and neurodegeneration: A review of literature, Pharmacol. Rep. 67 (2015) 970–979. https://doi.org/10.1016/j.pharep.2015.03.002.

[34] M. Huang, X. Jiang, Y. Liang, Q. Liu, S. Chen, Y. Guo, Berberine improves cognitive impairment by promoting autophagic clearance and inhibiting production of β-amyloid in APP/tau/PS1 mouse model of Alzheimer's disease, Exp. Gerontol. 91 (2017) 25–33. https://doi.org/10.1016/j.exger.2017.02.004.

[35] W. He, C. Wang, Y. Chen, Y. He, Z. Cai, Berberine attenuates cognitive impairment and ameliorates tau hyperphosphorylation by limiting the self-perpetuating pathogenic cycle between NF-κB signaling, oxidative stress and neuroinflammation, Pharmacol. Rep. 69 (2017) 1341–1348. https://doi.org/10.1016/j.pharep.2017.06.006.

[36] H.M. Hussien, A. Abd-Elmegied, D.A. Ghareeb, H.S. Hafez, H.E.A. Ahmed, N.A. El-moneam, Neuroprotective effect of berberine against environmental heavy metals-induced neurotoxicity and Alzheimer's-like disease in rats, Food Chem. Toxicol. 111 (2018) 432–444. https://doi.org/10.1016/j.fct.2017.11.025.

[37] T. Tarrago, N. Kichik, J. Seguí, E. Giralt, The Natural Product Berberine is a Human Prolyl Oligopeptidase Inhibitor, ChemMedChem. 2 (2007) 354–359. https://doi.org/10.1002/cmdc.200600303.

[38] B. Hille, E. Dickson, M. Kruse, B. Falkenburger, Chapter Ten - Dynamic Metabolic Control of an Ion Channel, in: K.T. Blackwell (Ed.), Prog. Mol. Biol. Transl. Sci., Academic Press, 2014: pp. 219–247. https://doi.org/10.1016/B978-0-12-397897-4.00008-5.

[39] S.H. Kim, S.J. Lee, J.H. Lee, W.S. Sun, J.H. Kim, Antimicrobial activity of 9-O-acyl- and 9-O-alkylberberrubine derivatives, Planta Med. 68 (2002) 277–281. https://doi.org/10.1055/s-2002-23128.

[40] K. Iwasa, M. Kamigauchi, M. Ueki, M. Taniguchi, Antibacterial activity and structure-activity relationships of berberine analogs, Eur. J. Med. Chem. 31 (1996) 469–478. https://doi.org/10.1016/0223-5234(96)85167-1.

[41] Y. Ding, X. Ye, J. Zhu, X. Zhu, X. Li, B. Chen, Structural modification of berberine alkaloid and their hypoglycemic activity, J. Funct. Foods. 7 (2014) 229–237. https://doi.org/10.1016/j.jff.2014.02.007.

[42] H. Jiang, X. Wang, L. Huang, Z. Luo, T. Su, K. Ding, X. Li, Benzenediol-berberine hybrids: Multifunctional agents for Alzheimer's disease, Bioorg. Med. Chem. 19 (2011) 7228–7235. https://doi.org/10.1016/j.bmc.2011.09.040.

[43] W.-J. Shan, L. Huang, Q. Zhou, F.-C. Meng, X.-S. Li, Synthesis, biological evaluation of 9-N-substituted berberine derivatives as multi-functional agents of antioxidant, inhibitors of acetylcholinesterase, butyrylcholinesterase and amyloid-β aggregation, Eur. J. Med. Chem. 46 (2011) 5885–5893. https://doi.org/10.1016/j.ejmech.2011.09.051.

[44] S. Zhang, X. Wang, W. Yin, Z. Liu, M. Zhou, D. Xiao, Y. Liu, D. Peng, Synthesis and hypoglycemic activity of 9-O-(lipophilic group substituted) berberine derivatives, Bioorg. Med. Chem. Lett. 26 (2016) 4799–4803. https://doi.org/10.1016/j.bmcl.2016.08.027.

[45] R. Li, J. Wu, Y. He, L. Hai, Y. Wu, Synthesis and in vitro evaluation of 12-(substituted aminomethyl) berberrubine derivatives as anti-diabetics, Bioorg. Med. Chem. Lett. 24 (2014). https://doi.org/10.1016/j.bmcl.2014.02.032.

[46] X. Li, D. Song, S.X. Leng, Link between type 2 diabetes and Alzheimer's disease: from epidemiology to mechanism and treatment, Clin. Interv. Aging. 10 (2015) 549–560. https://doi.org/10.2147/CIA.S74042.

[47] X. Bian, L. He, G. Yang, Synthesis and antihyperglycemic evaluation of various protoberberine derivatives, Bioorg. Med. Chem. Lett. 16 (2006) 1380–1383. https://doi.org/10.1016/j.bmcl.2005.11.045.

[48] G.-Y. Pan, Z.-J. Huang, G.-J. Wang, J.P. Fawcett, X.-D. Liu, X.-C. Zhao, J.-G. Sun, Y.-Y. Xie, The antihyperglycaemic activity of berberine arises from a decrease of glucose absorption, Planta Med. 69 (2003) 632–636. https://doi.org/10.1055/s-2003-41121.

[49] J. Yin, R. Hu, M. Chen, J. Tang, F. Li, Y. Yang, J. Chen, Effects of berberine on glucose metabolism in vitro, Metabolism. 51 (2002) 1439–1443. https://doi.org/10.1053/meta.2002.34715.

[50] Y. Wang, J.A. Zidichouski, Update on the Benefits and Mechanisms of Action of the Bioactive Vegetal Alkaloid Berberine on Lipid Metabolism and Homeostasis, Cholesterol. (2018). https://doi.org/10.1155/2018/7173920.

[51] H.S. Bodiwala, S. Sabde, D. Mitra, K.K. Bhutani, I.P. Singh, Synthesis of 9-substituted derivatives of berberine as anti-HIV agents, Eur. J. Med. Chem. 46 (2011) 1045–1049. https://doi.org/10.1016/j.ejmech.2011.01.016.

[52] G.L. Ellman, K.D. Courtney, V. Andres, R.M. Feather-Stone, A new and rapid colorimetric determination of acetylcholinesterase activity, Biochem. Pharmacol. 7 (1961) 88–95.

[53] S. Mak, W.W.K. Luk, W. Cui, S. Hu, K.W.K. Tsim, Y. Han, Synergistic inhibition on acetylcholinesterase by the combination of berberine and palmatine originally isolated from Chinese medicinal herbs, J. Mol. Neurosci. MN. 53 (2014) 511–516. https://doi.org/10.1007/s12031-014-0288-5.

[54] O. Soukup, D. Jun, J. Zdarova-Karasova, J. Patocka, K. Musilek, J. Korabecny, J. Krusek, M. Kaniakova, V. Sepsova, J. Mandikova, F. Trejtnar, M. Pohanka, L. Drtinova, M. Pavlik, G. Tobin, K. Kuca, A resurrection of 7-MEOTA: a comparison with tacrine, Curr. Alzheimer Res. 10 (2013) 893–906.

[55] M. Roselli, M.M. Cavalluzzi, C. Bruno, A. Lovece, A. Carocci, C. Franchini, S. Habtemariam, G. Lentini, Synthesis and evaluation of berberine derivatives and analogs as potential antiacetylcholinesterase and antioxidant agents, Phytochem. Lett. 18 (2016) 150–156. https://doi.org/10.1016/j.phytol.2016.10.005.

[56] L. Huang, A. Shi, F. He, X. Li, Synthesis, biological evaluation, and molecular modeling of berberine derivatives as potent acetylcholinesterase inhibitors, Bioorg. Med. Chem. 18 (2010) 1244–1251. https://doi.org/10.1016/j.bmc.2009.12.035.

[57] E. Giacobini, Selective inhibitors of butyrylcholinesterase: a valid alternative for therapy of Alzheimer's disease?, Drugs Aging. 18 (2001) 891–898.

[58] P.T. Männisto, J. Venäläinen, A. Jalkanen, J.A. García-Horsman, Prolyl oligopeptidase: a potential target for the treatment of cognitive disorders, Drug News Perspect. 20 (2007) 293–305. https://doi.org/10.1358/dnp.2007.20.5.1120216.

[59] K.S. Laitinen, T. van Groen, H. Tanila, J. Venäläinen, P.T. Männistö, I. Alafuzoff, Brain prolyl oligopeptidase activity is associated with neuronal damage rather than beta-amyloid accumulation, Neuroreport. 12 (2001) 3309–3312. https://doi.org/10.1097/00001756-200110290-00032.

[60] T. Tarrago, N. Kichik, J. Seguí, E. Giralt, The Natural Product Berberine is a Human Prolyl Oligopeptidase Inhibitor, ChemMedChem. 2 (2007) 354–359. https://doi.org/10.1002/cmdc.200600303.

[61] J. Cheung, M.J. Rudolph, F. Burshteyn, M.S. Cassidy, E.N. Gary, J. Love, M.C. Franklin, J.J. Height, Structures of human acetylcholinesterase in complex with pharmacologically important ligands, J. Med. Chem. 55 (2012) 10282–10286. https://doi.org/10.1021/jm300871x.

[62] F. Nachon, E. Carletti, C. Ronco, M. Trovaslet, Y. Nicolet, L. Jean, P.-Y. Renard, Crystal structures of human cholinesterases in complex with huprine W and tacrine: elements of specificity for anti-Alzheimer's drugs targeting acetyl- and butyryl-cholinesterase, Biochem. J. 453 (2013) 393–399. https://doi.org/10.1042/BJ20130013.

[63] C.D. Haffner, C.J. Diaz, A.B. Miller, R.A. Reid, K.P. Madauss, A. Hassell, M.H. Hanlon, D.J.T. Porter, J.D. Becherer, L.H. Carter, Pyrrolidinyl pyridone and pyrazinone analogues as potent inhibitors of prolyl oligopeptidase (POP), Bioorg. Med. Chem. Lett. 18 (2008) 4360–4363. https://doi.org/10.1016/j.bmcl.2008.06.067.

[64] C.-G. Zhan, D. Gao, Catalytic Mechanism and Energy Barriers for Butyrylcholinesterase-Catalyzed Hydrolysis of Cocaine, Biophys. J. 89 (2005) 3863–3872. https://doi.org/10.1529/biophysj.105.070276.

[65] J.A. García-Horsman, P.T. Männistö, J.I. Venäläinen, On the role of prolyl oligopeptidase in health and disease, Neuropeptides. 41 (2007) 1–24. https://doi.org/10.1016/j.npep.2006.10.004.

[66] K. Kánai, P. Arányi, Z. Böcskei, G. Ferenczy, V. Harmat, K. Simon, S. Bátori, G. Náray-Szabo, I. Hermecz, Prolyl oligopeptidase inhibition by N-acyl-pro-pyrrolidine-type molecules, J. Med. Chem. 51 (2008) 7514–7522. https://doi.org/10.1021/jm800944x.

[67] O. Soukup, R. Dolezal, D. Malinak, J. Marek, S. Salajkova, M. Pasdiorova, J. Honegr, J. Korabecny, P. Nachtigal, F. Nachon, D. Jun, K. Kuca, Synthesis, antimicrobial evaluation and molecular modeling of 5-hydroxyisoquinolinium salt series; the effect of the hydroxyl moiety., Bioorg. Med. Chem. 24 (2016) 841–848. https://doi.org/10.1016/j.bmc.2016.01.006.

[68] J. van Meerloo, G.J.L. Kaspers, J. Cloos, Cell sensitivity assays: the MTT assay, Methods Mol. Biol. Clifton NJ. 731 (2011) 237–245. https://doi.org/10.1007/978-1-61779-080-5_20.

[69] P. Molyneux, The use of the stable free radical diphenylpicryl- hydrazyl (DPPH) for estimating antioxidant activity, 26 (2004) 9.

[70] V. Pongkittiphan, W. Chavasiri, R. Supabphol, Antioxidant Effect of Berberine and its Phenolic Derivatives Against Human Fibrosarcoma Cells, Asian Pac. J. Cancer Prev. APJCP. 16 (2015) 5371–5376. https://doi.org/10.7314/apjcp.2015.16.13.5371.

[71] P. Chetia, A. Bala, B. Khandelwal, P. Haldar, Comparative in vitro Free Radical Scavenging Property of -carotene and Naringenin with Respect to Vitamin C and N-acetyl Cysteine, Pharmacologia. 3 (2012) 724–728. https://doi.org/10.5567/pharmacologia.2012.724.728.

[72] Z. Chen, R. Bertin, G. Froldi, EC50 estimation of antioxidant activity in DPPH assay using several statistical programs, Food Chem. 138 (2013) 414–420. https://doi.org/10.1016/j.foodchem.2012.11.001.

[73] R.D. Faitanin, J.V.D. Gomes, L.F.T. Menezes, Á.C. Neto, R. de C.R. Gonçalves, R.R. Kitagawa, D. Silveira, C.M. Jamal, Chemical study and evaluation of antioxidant activity and α-glucosidase inhibition of Myrciaria strigipes O. Berg (Myrtaceae) -, J. Appl. Pharm. Sci. 8 (2018) 120–125.

[74] J.A. Hardy, G.A. Higgins, Alzheimer's disease: the amyloid cascade hypothesis, Science. 256 (1992) 184–185.

[75] L. Tran, T. Ha-Duong, Exploring the Alzheimer amyloid-β peptide conformational ensemble: A review of molecular dynamics approaches, Peptides. 69 (2015) 86–91. https://doi.org/10.1016/j.peptides.2015.04.009.

[76] R. Franco, A. Cedazo-Minguez, Successful therapies for Alzheimer's disease: why so many in animal models and none in humans?, Front. Pharmacol. 5 (2014) 146. https://doi.org/10.3389/fphar.2014.00146.

[77] M. Asai, N. Iwata, A. Yoshikawa, Y. Aizaki, S. Ishiura, T.C. Saido, K. Maruyama, Berberine alters the processing of Alzheimer's amyloid precursor protein to decrease Aβ secretion, Biochem. Biophys. Res. Commun. 352 (2007) 498–502. https://doi.org/10.1016/j.bbrc.2006.11.043.

[78] A. Gautieri, M. Beeg, M. Gobbi, F. Rigoldi, L. Colombo, M. Salmona, The Anti-Amyloidogenic Action of Doxycycline: A Molecular Dynamics Study on the Interaction with Aβ42, Int. J. Mol. Sci. 20 (2019). https://doi.org/10.3390/ijms20184641.

[79] I. Grundke-Iqbal, K. Iqbal, Y.C. Tung, M. Quinlan, H.M. Wisniewski, L.I. Binder, Abnormal phosphorylation of the microtubule-associated protein tau (tau) in Alzheimer cytoskeletal pathology, Proc. Natl. Acad. Sci. U. S. A. 83 (1986) 4913–4917. https://doi.org/10.1073/pnas.83.13.4913.

[80] J.T. Pedersen, E.M. Sigurdsson, Tau immunotherapy for Alzheimer's disease, Trends Mol. Med. 21 (2015) 394–402. https://doi.org/10.1016/j.molmed.2015.03.003.

[81] L. Di, E.H. Kerns, K. Fan, O.J. McConnell, G.T. Carter, High throughput artificial membrane permeability assay for blood–brain barrier, Eur. J. Med. Chem. 38 (2003) 223–232. https://doi.org/10.1016/S0223-5234(03)00012-6.

[82] L.F.N. Lemes, G. de Andrade Ramos, A.S. de Oliveira, F.M.R. da Silva, G. de Castro Couto, M. da Silva Boni, M.J.R. Guimarães, I.N.O. Souza, M. Bartolini, V. Andrisano, P.C. do Nascimento Nogueira, E.R. Silveira, G.D. Brand, O. Soukup, J. Korábečný, N.C. Romeiro, N.G. Castro, M.L. Bolognesi, L.A.S. Romeiro, Cardanol-derived AChE inhibitors: Towards the development of dual binding derivatives for Alzheimer's disease, Eur. J. Med. Chem. 108 (2016) 687–700. https://doi.org/10.1016/j.ejmech.2015.12.024.

[83] X. Wang, R. Wang, D. Xing, H. Su, C. Ma, Y. Ding, L. Du, Kinetic difference of berberine between hippocampus and plasma in rat after intravenous administration of Coptidis rhizoma extract, Life Sci. 77 (2005) 3058–3067. https://doi.org/10.1016/j.lfs.2005.02.033.

[84] C. Li, S. Wainhaus, A.S. Uss, K.-C. Cheng, High-Throughput Screening Using Caco-2 Cell and PAMPA Systems, in: C. Ehrhardt, K.-J. Kim (Eds.), Drug Absorpt. Stud. Situ Vitro Silico Models, Springer US, Boston, MA, 2008: pp. 418–429. https://doi.org/10.1007/978-0-387-74901-3_18.

[85] M. Imenshahidi, H. Hosseinzadeh, Berberine and barberry (Berberis vulgaris): A clinical review, Phytother. Res. 33 (2019) 504–523. https://doi.org/10.1002/ptr.6252.

[86] R.R. Ramsay, M.R. Popovic-Nikolic, K. Nikolic, E. Uliassi, M.L. Bolognesi, A perspective on multi-target drug discovery and design for complex diseases, Clin. Transl. Med. 7 (2018). https://doi.org/10.1186/s40169-017-0181-2.

[87] B.M. Mistry, R.V. Patel, Y.-S. Keum, D.H. Kim, Synthesis of 9-O-3-(1-piperazinyl/morpholinyl/piperidinyl)pentyl-berberines as Potential Antioxidant and Cytotoxic Agents, Anticancer Agents Med. Chem. 16 (2016) 713–721.

[88] E.F. Pettersen, T.D. Goddard, C.C. Huang, G.S. Couch, D.M. Greenblatt, E.C. Meng, T.E. Ferrin, UCSF Chimera--a visualization system for exploratory research and analysis, J. Comput. Chem. 25 (2004) 1605–1612. https://doi.org/10.1002/jcc.20084.

[89] J. Cheung, M.J. Rudolph, F. Burshteyn, M.S. Cassidy, E.N. Gary, J. Love, M.C. Franklin, J.J. Height, Structures of human acetylcholinesterase in complex with pharmacologically important ligands, J. Med. Chem. 55 (2012) 10282–10286. https://doi.org/10.1021/jm300871x.

[90] F. Nachon, E. Carletti, C. Ronco, M. Trovaslet, Y. Nicolet, L. Jean, P.-Y. Renard, Crystal structures of human cholinesterases in complex with huprine W and tacrine: elements of specificity for anti-Alzheimer's drugs targeting acetyl- and butyryl-cholinesterase, Biochem. J. 453 (2013) 393–399. https://doi.org/10.1042/BJ20130013.

[91] C.D. Haffner, C.J. Diaz, A.B. Miller, R.A. Reid, K.P. Madauss, A. Hassell, M.H. Hanlon, D.J.T. Porter, J.D. Becherer, L.H. Carter, Pyrrolidinyl pyridone and pyrazinone analogues as potent inhibitors of prolyl oligopeptidase (POP), Bioorg. Med. Chem. Lett. 18 (2008) 4360–4363. https://doi.org/10.1016/j.bmcl.2008.06.067.

[92] M.D. Hanwell, D.E. Curtis, D.C. Lonie, T. Vandermeersch, E. Zurek, G.R. Hutchison, Avogadro: an advanced semantic chemical editor, visualization, and analysis platform, J. Cheminformatics. 4 (2012) 17. https://doi.org/10.1186/1758-2946-4-17.

[93] O. Trott, A.J. Olson, AutoDock Vina: improving the speed and accuracy of docking with a new scoring function, efficient optimization and multithreading, J. Comput. Chem. 31 (2010) 455–461. https://doi.org/10.1002/jcc.21334.

[94] B. Liu, L. Wang, Y.-H. Jin, An effective PSO-based memetic algorithm for flow shop scheduling, IEEE Trans. Syst. Man Cybern. Part B Cybern. Publ. IEEE Syst. Man Cybern. Soc. 37 (2007) 18–27.

[95] K. Bentayeb, C. Rubio, C. Nerín, Study of the antioxidant mechanisms of Trolox and eugenol with 2,2'-azobis(2-amidinepropane)dihydrochloride using ultra-high performance liquid chromatography coupled with tandem mass spectrometry, The Analyst. 137 (2012) 459–470. https://doi.org/10.1039/c1an15505a.

[96] Y. Pan, Y. Chen, Q. Li, X. Yu, J. Wang, J. Zheng, The Synthesis and Evaluation of Novel Hydroxyl Substituted Chalcone Analogs with in Vitro Anti-Free Radicals Pharmacological Activity and in Vivo Anti-Oxidation Activity in a Free Radical-Injury Alzheimer's Model, Molecules. 18 (2013) 1693–1703. https://doi.org/10.3390/molecules18021693.

[97] A. Gandini, M. Bartolini, D. Tedesco, L. Martinez-Gonzalez, C. Roca, N.E. Campillo, J. Zaldivar-Diez, C. Perez, G. Zuccheri, A. Miti, A. Feoli, S. Castellano, S. Petralla, B. Monti, M. Rossi, F. Moda, G. Legname, A. Martinez, M.L. Bolognesi, Tau-Centric Multitarget Approach for Alzheimer's Disease: Development of First-in-Class Dual Glycogen Synthase Kinase 3β and Tau-Aggregation Inhibitors, J. Med. Chem. 61 (2018) 7640–7656. https://doi.org/10.1021/acs.jmedchem.8b00610.

[98] L. Di, E.H. Kerns, K. Fan, O.J. McConnell, G.T. Carter, High throughput artificial membrane permeability assay for blood-brain barrier, Eur. J. Med. Chem. 38 (2003) 223–232.

[99] Y. Zhang, M. Huo, J. Zhou, S. Xie, PKSolver: An add-in program for pharmacokinetic and pharmacodynamic data analysis in Microsoft Excel, Comput. Methods Programs Biomed. 99 (2010) 306–314. https://doi.org/10.1016/j.cmpb.2010.01.007.

Highlights:

- The set of novel 22 berberine derivatives was prepared
- Hybrids exhibited multi-targeted profile with potential to treat Alzheimer's disease
- Compounds revealed balanced inhibition properties against prolyl oligopeptidase and cholinesterases in micromolar range
- The docking simulation predicted their binding modes into the active sites of the mentioned enzymes
- Top-ranked compounds exerted anti-amyloid and anti-tau properties

Declaration of interests

☒ The authors declare that they have no known competing financial interests or personal relationships that could have appeared to influence the work reported in this paper.

☒The authors declare the following financial interests/personal relationships which may be considered as potential competing interests: